Life-long epigenetic programming of cortical architecture by maternal 'Western' diet during pregnancy

Valentina Cinquina[1], Daniela Calvigioni[1], Matthias Farlik[2], Florian Halbritter[2], Victoria Gernedl[2], Sally L. Shirran[3], Matthew A. Fuszard[3,$], Catherine H. Botting[3], Patrick Poullet[4], Fabiana Piscitelli[5], Zoltán Máté[6], Gábor Szabó[6], Yuchio Yanagawa[7], Siegfried Kasper[8], Vincenzo Di Marzo[5,9], Ken Mackie[10], Chris J. McBain[11], Christoph Bock[2,12], Erik Keimpema[1] and Tibor Harkany[1,13,#]

[1]Department of Molecular Neurosciences, Center for Brain Research, Medical University of Vienna, Vienna, Austria,
[2]CeMM Research Center for Molecular Medicine of the Austrian Academy of Sciences, Vienna, Austria,
[3]School of Chemistry, University of St. Andrews, St. Andrews, United Kingdom,
[4]Institut Curie & INSERM U900, Paris, France,
[5]Endocannabinoid Research Group, Institute of Biomolecular Chemistry (ICB), National Research Council (CNR), Pozzuoli, Italy,
[6]Institute of Experimental Medicine, Hungarian Academy of Sciences, Budapest, Hungary,
[7]Department of Genetic and Behavioral Neuroscience, Gunma University School of Medicine, Maebashi, Japan,
[8]Department of Psychiatry and Psychotherapy, Medical University of Vienna, Vienna, Austria,
[9]Canada Excellence Research Chair, Institut Universitaire de Cardiologie et de Pneumologie de Québec and Institut sur la Nutrition et les Aliments Fonctionnels, Université Laval, Québec, QC, Canada,
[10]Department of Psychological & Brain Sciences, Indiana University, Bloomington, Indiana, USA,
[11]Program in Developmental Neuroscience, Eunice Kennedy-Shriver National Institute of Child Health and Human Development, NIH, Bethesda, USA,
[12]Department of Laboratory Medicine, Medical University of Vienna, Vienna, Austria,
[13]Department of Neuroscience, Karolinska Institutet, Stockholm, Sweden.

[$]*Present address*: Faculty of Medicine, Martin-Luther University, Halle-Wittenberg, Halle, Germany

[#]*Correspondence to:* **Dr. Tibor Harkany**, Department of Molecular Neurosciences, Center for Brain Research, Medical University of Vienna, Spitalgasse 4, A-1090 Vienna, Austria. *Tel:* +43 1 40160 34050; *Fax:* +43 1 40160 934063; *e-mail*: Tibor.Harkany@meduniwien.ac.at

Abstract

The evolution of human diets led to preferences towards polyunsaturated fatty acid (PUFA) content with 'Western' diets enriched in ω-6 PUFAs. Mounting evidence points to ω-6 PUFA excess limiting metabolic and cognitive processes that define longevity in humans. When chosen during pregnancy, ω-6 PUFA-enriched 'Western' diets can reprogram maternal bodily metabolism with maternal nutrient supply precipitating the body-wide imprinting of molecular and cellular adaptations at the level of long-range intercellular signaling networks in the unborn fetus. Even though unfavorable neurological outcomes are amongst the most common complications of intrauterine ω-6 PUFA excess, cellular underpinnings of life-long modifications to brain architecture remain unknown. Here, we show that nutritional ω-6 PUFA-derived endocannabinoids desensitize CB_1 cannabinoid receptors, thus inducing epigenetic repression of transcriptional regulatory networks controlling neuronal differentiation. We found that cortical neurons lose their positional identity and axonal selectivity when mouse fetuses are exposed to excess ω-6 PUFAs *in utero*. Conversion of ω-6 PUFAs into endocannabinoids disrupted the temporal precision of signaling at neuronal CB_1 cannabinoid receptors, chiefly deregulating *Stat3*-dependent transcriptional cascades otherwise required to execute neuronal differentiation programs. Global proteomics identified the immunoglobulin family of cell adhesion molecules (IgCAMs) as direct substrates, with DNA methylation and chromatin accessibility profiling uncovering epigenetic reprogramming at >1,400 sites in neurons after prolonged cannabinoid exposure. We found anxiety and depression-like behavioral traits to manifest in adult offspring, which is consistent with genetic models of reduced IgCAM expression, to suggest causality for cortical wiring defects. Overall, our data uncover a regulatory mechanism whose disruption by maternal food choices could limit an offspring's brain function for life.

Introduction

Establishing the cerebral connectome relies on mechanisms that produce unique topological specificity for each neuron to receive up to 30-40,000 synapses (1) for information exchange. Pyramidal cells and GABA interneurons, modulated by subcortical afferents, construct cortical microcircuits that represent the cellular backbones of high-order integrative processes. During the fetal period, telencephalic stem cell pools contribute neurons to the cerebral cortex (2, 3): neuroblasts engage in long-distance migration along complex trajectories for layer-specific homing before their terminal morphogenesis, including the specification and directional growth of their axons, can commence (2). These developmental stages are controlled by intercellular signals (including activity-dependence, morphogens and

chemotaxic cues) that engage transcriptional differentiation programs intracellularly to define neuronal identity (3).

Fetal development relies on sequential cell divisions that generate tissue mass and topological specificity for which nutrients are transferred along maternal-placental-fetal nutrient interfaces (2). A critical metabolic demand for both cell division and morphological differentiation is the availability of membrane lipid precursors to envelop developing cells. Accordingly, about half of the dry weight of the brain is made up by lipids, of which 20-25% are long-chain polyunsaturated fatty acids (PUFAs) (4), with 20:4 ω-6 arachidonic acid (AA) being a prominent constituent. Incorporation of long-chain PUFAs into biological membranes allows for well-controlled membrane expansion as axons and dendrites form (5). They also play important roles in trans-membrane transport and receptor-dependent second messenger signaling (4). Significantly, AA also serves as the ultimate precursor to eicosanoids, including their non-classical endocannabinoid subfamily (6): *i*) *sn*-2-AA containing diacylglycerols, which are cleaved by *sn*-1-diacylglycerol lipases to generate 2-arachydonoylglycerol (2-AG; *sn* designation for stereospecific numbering by convention; (7)), or *ii*) *N*-arachidonoyl-phosphatidylethanolamine (NAPE), which is cleaved by a NAPE-selective phospholipase D to generate *N*-arachidonoylethanolamine (anandamide, AEA; (6, 8)). Significantly, 2-AG in the developing brain engages CB_1 cannabinoid receptors (CB_1Rs) on neurons to act as repulsive guidance cue for cell migration (9) and to inhibit neurite outgrowth and morphogenesis (9, 10) (**Fig. S1a,b**). Despite these inferences, causality between maternal PUFA metabolism and the (de-)regulation of local-acting instructive lipid signals indispensable for cortical development (4) and influencing neurodevelopmental outcomes has not been established.

The bulk of fetal PUFAs (including AA) available for signaling and in lipid depots are of maternal origin, despite fetal lipogenesis becoming progressively operational from mid-gestation (11). Accordingly, maternal dietary choices commonly impact birth weight, neurological status, postnatal cognition and life expectancy in both humans and rodent models (11). Medical guidelines highlight maternal food intake during pregnancy as a major factor for child development with a near-equivalent ratio of ω-3 (rich in fish and 'Japanese' diet) and ω-6 PUFAs recommended as dietary optimum (12) to satisfy basic metabolic demands by sustained precursor availability and to prevent adverse neurological outcomes (13). However, with more than 30% of children born to overweight/obese mothers (14); a dramatic deviation from this dietary optimum likely exists for prolonged periods, as either the relative or the total amount of ω-6 PUFAs being in excess (15). Therefore, 'Western' diets

rich in ω-6 PUFA precursors are likely to be detrimental for intrauterine development (14). The consumption of ω-6 PUFA-rich diets prior to conception is equally alarming since the composition of pre-existing maternal fat depots that undergo accelerated breakdown during the last trimester of pregnancy (14) determine the molecular diversity of bioactive lipid precursors for the fetus as it develops. Moreover, in both humans and rodents (16, 17) high-fat diets increase AA in the circulation that in turn increases the availability of endocannabinoids and, consequently, modulates the function of the endocannabinoid system (15). Yet a mechanistic and causal relationship between a shift towards maternal ω-6 PUFA preference (even if retaining a relative ω-3:ω-6 PUFA ratio) and life-long neurodevelopmental deficits that render the offspring's nervous system prone to postnatal maladaptation remains unknown.

Materials & Methods

Animals, feeding regime and tissue collection. Female C57Bl6/J, cholecystokinin $(CCK)^{BAC/DsRed}$ and $CCK^{BAC/DsRed}$::$GAD67^{gfp/+}$ transgenic mice (18) were housed in groups in clear plastic cages on a 12h/12h light/dark cycle (lights on at 08:00 h) and in a temperature (22 ± 2 °C) and humidity (50 ± 10%)-controlled environment. Food and water were available *ad libitum*. Embryos and tissues were obtained from timed matings with the day of vaginal plug considered as embryonic day (E) 0.5. The day of birth was always registered as postnatal day (P) 0. Groups sizes conformed to those used as convention in developmental biology (10, 19-21).

Female animals at 6 weeks of age were randomly assigned to either a hypercaloric diet enriched ~15-fold in ω-6 PUFAs while maintaining the ω-3:ω-6 PUFA ratio at 1:8 as in standard chow or to a standard diet (**Fig. S2a-b$_1$** and **Table S1**). Diets were from Special Diet Services (United Kingdom) and quality controlled by mass-spectrometry. Maternal body weight was recorded 2-3 times per week for the duration of each study (**Fig. S2c**). The effect of maternal diets on fetal brain development was evaluated at E18.5 after both the '*priming protocol*' (consuming a high ω-6 PUFA diet starting 2 weeks prior to conception; **Fig. S2b**) or '*programming protocol*' (consuming a high ω-6 PUFA diet 8 weeks prior to conception, **Fig. S2b$_1$**). This experimental approach, which precluded blinding the investigators, was motivated by *i*) the switch of diets inducing transient changes in appetite and even loss of body weight, which, if occurring acutely could have biased fetal development and *ii*) changes in copulatory behaviors affecting both males and females on the first days of being exposed

to the modified diet. Moreover, long-lasting postnatal effects of maternal ω-6 PUFA-enriched diets were determined in adult offspring on P75.

Embryos were collected from $n \geq 5$ pregnancies to keep the number of independent observations sufficient for statistical analyses, sexed if appropriate, and used for histochemistry, proteomics, lipid analysis and molecular biology. The use of specific or mixed genders for particular experiments was specified. Embryos were collected by Cesarean sections from mothers anesthetized by isoflurane (5%, 1 L/min flow rate), weighed and decapitated with their heads either immersed in 4% paraformaldehyde (PFA) in 0.1 M Na^+ phosphate buffer (PB; pH 7.4) overnight or snap-frozen in liquid N_2 and stored at -80 °C until further processing (10, 18). Likewise, adult offspring were anesthetized in isoflurane (5%, 1 L/min flow rate), decapitated, with their brain tissues snap-frozen in liquid N_2 and stored at -80 °C.

Ethical approval of animal studies. Experiments on live animals conformed to the 2010/63/EU European Communities Council Directive and were approved by the Austrian Ministry of Science and Research (66.009/0145-WF/II/3b/2014, and 66.009/0277-WF/V/3b/2017). Particular effort was directed towards minimizing the number of animals used and their suffering during experiments.

Click-iT EdU labelling. Embryos were exposed to a single maternal intraperitoneal injection of 5-ethynyl-2'-deoxyuridine (EdU, 33 mg/kg) at E14.5 (in the '*programming protocol*' only). At E18.5, male embryos were selected by PCR genotyping (see Ref. (19) for primer pairs and protocol). Embryonic brains were immersion fixed in 4% PFA in PB overnight, rinsed in PB and cryoprotected in 30% sucrose (in PB) for 48 h. Serial coronal sections (20 μm) were cut on a ThermoFisher NX70 cryostat, thaw-mounted onto fluorescence-free SuperFrost$^+$ glass slides and stored at -20°C until processing. EdU was visualized with Alexa 488-azide using the Click-iT labeling technology (Life Technologies) (22).

Immunohistochemistry and quantitative morphometry. Immunofluorescence histochemistry was performed according to published protocols (10, 18, 19). Briefly, sections were extensively rinsed in PB and subsequently exposed to a blocking solution consisting of 5% normal donkey serum (NDS; Jackson ImmunoResearch), 1% bovine serum albumin (BSA; Sigma), and 0.3% Triton X-100 (Sigma) in PB for 2 h at 21-24°C. Next, sections were incubated with either anti-neural cell adhesion molecule L1 (L1CAM; 1:1,000, #ABT143, Millipore), or anti-Ki67 (which marks proliferation/early neuroblasts; 1:100, #AB9260,

Millipore) primary antibody diluted in PB also containing 0.1% NDS and 0.3% Triton X-100 at 4°C for 48 h. Limbic system associated membrane protein (LSAMP) was localized to cortical territories of male $CCK^{BAC/DsRed}$ transgenic mice at E18.5 by first exposing glass-mounted coronal sections to a 0.1 M Tris-glycine solution (pH 7.4; Sigma) at 21-24 ^{o}C for 20 min. After rinsing in 0.05 M phosphate-buffered saline (PBS), sections were incubated with mouse anti-LSAMP primary antibody (1:50; #2G9, Developmental Studies Hybridoma Bank) for 48h (Dr. Pimenta Aurea's suggestions for histochemistry are greatly acknowledged). DyLight Fluor 488-tagged secondary antibodies (1:300; Jackson ImmunoResearch) were used to reveal the localization of primary antibodies. Sections were coverslipped with Aquamount (Dako). Images were acquired on Zeiss 700LSM and 880LSM confocal laser scanning microscopes. Multi-panel images were assembled in CorelDRAW X7 (Corel Corp.).

Axonal morphometry was performed as described earlier (10, 19). In brief, the diameter of first-order bundles made up by corticofugal axons on E18.5 was measured in serial sections of 20 µm thickness that had been cut and processed as above. The number of immunoreactive or genetically-tagged neurons in the fetal cerebral cortex was determined using equivalent and binned surface areas, and expressed as absolute values.

Liquid chromatography-atmospheric pressure chemical ionization mass spectrometry. Extraction, purification, and quantification of 2-AG and AEA from cortical tissues of E18.5 embryos and P75 mice (for embryos also including dorsal hippocampus) fed with either hypercaloric or standard diet were carried out according to published protocols (23, 24). Briefly, tissues were rapidly dissected out, snap-frozen in liquid N_2 and stored at -80 °C. After lipid extraction and prepurification on silica gel columns, 2-AG and AEA levels from *n* = 3 animals/condition were determined by isotope dilution using liquid chromatography-atmospheric pressure chemical ionization mass spectrometry (Shimadzu LCMS-2020). Results were expressed as pmol/mg of tissue.

iTRAQ proteomics. Single cortical hemispheres (*n* = 6/group, mixed and balanced for sex from independent pregnancies) were obtained from E18.5 fetuses. Contralateral hemispheres were snap frozen for target validation by quantitative real-time PCR and/or Western blotting (*see below*). Proteins were extracted by homogenization in lysis buffer (pH 10.0) of triethylammonium bicarbonate (25 mM, Sigma), Na_2CO_3 (20 mM, Sigma) in the presence of protease inhibitors (cocktail; Sigma). Protein concentrations were determined by the bicinchoninic acid assay (BCA; ThermoFisher). After quantification, proteins were

precipitated in 6 volumes of ice-cold acetone. One hundred µg of proteins per sample were used for isobaric tagging for relative and absolute quantitation (iTRAQ) in an 8-plex layout per the manufacturer's instructions (ABSciex). In brief, proteins were denatured, reduced, alkylated, trypsin digested (Promega), individually labeled with appropriate iTRAQ tags, pooled, concentrated, re-suspended in 1.4 ml loading buffer (10 mM KH_2PO_4 pH 3.0 in 25% acetonitrile) and sonicated.

Peptides were separated by cation exchange chromatography on a PolySulfoethyl A column (PolyLC) over 30 min with a KCl gradient increasing up to 0.5 M, and 0.5 ml fractions collected. Fifteen fractions across the elution profile of similar peptide concentration were generated and concentrated (SpeedVac). Fractions were re-suspended in 0.1% trifluoroacetic acid (TFA) and desalted on C18 spin columns (PepClean C18, Thermo Scientific). Half of each fraction was then injected on an Acclaim PepMap 100 C18 trap and an Acclaim PepMap RSLC C18 column (ThermoFisher), using a nanoLC Ultra 2D plus loading pump and nanoLC as-2 autosampler (Eksigent). The peptides were loaded onto the trap in a mixture of 98% water, 2% acetonitrile and 0.05% TFA, and washed for 20 min to waste before switching in line with the column and were then eluted with a gradient of increasing acetonitrile, containing 0.1 % formic acid (2-20% acetonitrile in 90 min, 20-40% in a further 30 min, followed by 98% acetonitrile to clean the column, before re-equilibration to 2% acetonitrile). The eluate was sprayed into a TripleTOF 5600 electrospray tandem mass spectrometer (ABSciex) and analyzed in Information Dependent Acquisition (IDA) mode, performing 120 ms of MS followed by 80 ms MSMS analyses on the 20 most intense peaks seen by MS, with the „Adjust Collision Energy when using iTRAQ reagent" box ticked in the method.

Data files were processed by ProteinPilot 4.5 (Sciex) using the Paragon algorithm, searching against the SwissProt database (March 2013 edition). The following settings were selected: *sample type*: iTRAQ 8-plex (peptide labelled), *cysteine alkylation*: MMTS, *digestion*: trypsin, *instrument*: TripleTOF 5600, *species*: mouse, *ID focus*: biological modifications and amino acid substitutions and *search effort*: thorough. Results files were exported to Microsoft Excel (**Table S2**), with statistical analysis in SPSS v. 21.

RNA isolation and quantitative PCR. RNA was extracted using the RNeasy mini kit (Qiagen) with a DNase I step performed to eliminate traces of genomic DNA. Total RNA was then reverse transcribed to a cDNA library in a reaction mixture using a high-capacity cDNA reverse transcription kit (Applied Biosystems). The cDNA library was then used for

quantitative real-time PCR (CFX-connect, Bio-Rad). Pairs of PCR primers specific for neural cell adhesion molecule L1 (*L1cam*), neural cell adhesion molecule 1 (*Ncam*), limbic system-associated membrane protein (*Lsamp*), neurotrimin (*Ntm*), cannabinoid receptor 1 (*Cnr1*), signal transducer and activator of transcription 3 (*Stat3*), myeloblastosis oncogene (*Myb*) and the CCAAT/enhancer-binding protein beta (*Cebpb*) were designed with Primer Bank and National Center for Biotechnology Information (NCBI) Primer Blast software (**Table S3**). Quantitative analysis of gene expression was performed with the SYBR Green Master Mix Kit (Life Technologies). Expression levels were normalized to the housekeeping gene encoding glyceraldehyde-3-phosphate dehydrogenase (*Gapdh*) for every sample in parallel assays.

Quantitative Western blotting with total protein normalization. Cerebral samples of E18.5 male embryos and postnatal mice (mixed for sex) were obtained as described above. Total protein labeling was initiated by adding carbocyanine (Cy)5 dye reagent (GE Healthcare) that had been pre-diluted (1:10) in ultrapure water. Samples were mixed and incubated for 5 min at 21-24 ^{o}C. The labeling reaction was terminated by adding Amersham WB loading buffer (GE Healthcare; 20 µl/sample) containing 40 µM DTT. Samples were then boiled at 95 °C for 3 min with equal amounts (20 µg/40 µl) and subsequently loaded onto an Amersham WB gel card (13.5%). Electrophoresis (600V, 42 min) and protein transfer onto polyvinylidine-difluoride membranes (100V, 30 min) were at default settings in an integrated Amersham WB system (GE Healthcare) for quantitative SDS-PAGE and Western blotting of proteins with fluorescence detection. After blocking, membranes were incubated with guinea pig anti-CB_1R antibody (1:500, kindly provided by Dr. Masahiko Watanabe) and mouse anti-LSAMP antibody (1:100; #2G9, Developmental Studies Hybridoma Bank) overnight. To demonstrate the specificity of the guinea pig anti-CB_1R antibody, we prepared cerebellar homogenates from wild-type and *Cnr1*$^{-/-}$ littermates. A specific band at the calculated molecular weight of this receptor (53 kDa) was detected in wild-type mice but not *Cnr1*$^{-/-}$ mice (*see Results below*). Antibody binding was detected by using species-specific (anti-mouse and anti-guinea pig) Cy3-labeled secondary antibodies (1:1,000; GE Healthcare). Membranes were dried before scanning at 560 nm (Cy3) and 630 nm (Cy5) excitation. Automated image analysis was performed with the Amersham WB evaluation software with manual optimization if necessary.

Behavioral tests. Anxiety-like behavior in the first generation offspring to dams fed with ω-6 PUFA-enriched or control chow were tested in the open-field and elevated plus maze (n = 6 male mice/group from independent pregnancies) as described (25, 26, 27). In the open-field

test, mice were allowed to explore a 50 × 50 cm arena for 5 minutes. The total distance travelled (m), their speed of movement (cm/s) and the time spent in an inner 15 cm-area (s) were measured. For the elevated plus maze, mice were placed in the center of a standard maze with its perpendicular arms measuring 10 × 50 cm each. Mice faced an open arm at start, and were allowed to explore the maze for 5 min. The distance travelled (cm) and the time spent (s) in the open and closed arms were measured and the number of arm entries (*n*) were determined. Parameters for the open arms (distance, time, entries) were expressed as the percentage of total arm entries.

Cultures of cortical neurons and IncuCyte-assisted neurite tracking. Cerebral tissues (cortex/hippocampus) of mouse embryos were isolated at E14.5 (mixed for sex) or E18.5 (males only). Cells were mechanically dissociated into single cell suspension by trypsin digestion (0.1%, 3 min) and plated at a density of 20,000 cells/well onto poly-D-lysine-coated (PDL; Sigma) 96-well plates. After 24h, cultures were exposed to 2-AG (5 µM; endocannabinoid and full CB_1R agonist), AA (10 µM; 2-AG precursor) or to AM251 (200 nM), an inverse CB_1R agonist, alone or in combination for 4 days (pharmacology) or 7 days (neurite outgrowth) (10,'20). Drug treatment was performed in quadruplicates with parallel live imaging on an IncuCyte Zoom live-cell imaging platform (Essen Bioscience). Time-lapse images were acquired every 2h. The growth rate of neurites in each well was determined as the surface area covered by neurites (soma free mode) and expressed as mm/mm^2 surface area. Surface occupancy of neurons after 4 days in culture was expressed as 'body cluster area' and expressed as percentage surface area covered by live neurons. This parameter was considered as a precise measure of cell survival.

DNA methylation. Extracted DNA was subjected to the reduced representation bisulfite sequencing (RRBS) workflow as described previously (28, 29): 100 ng of DNA were digested at 37°C for 12h with 20 units of MspI and TaqI (New England Biolabs) in 30 µl of 1x NEB buffer. Fill-in and A-tailing were performed by addition of Klenow Fragment 3' > 5' exo- (New England Biolabs) and dNTP mix (10 mM dATP, 1 mM dCTP, 1 mM dGTP). After ligation to methylated Illumina TruSeq LT v2 adaptors using Quick Ligase (New England Biolabs), the libraries were size selected by performing a 0.75x clean-up with AMPure XP beads (Beckman Coulter). The libraries were pooled in equal amounts based on qPCR data and bisulfite converted using the EZ DNA Methylation Direct Kit (Zymo Research). Bisulfite-converted libraries were enriched and quality control was performed using Qubit dsDNA HS (Life Technologies) and fragment length was assessed using high sensitivity DNA chips on a Bioanalyzer 2000 (Agilent). Sequencing was performed on an

Illumina HiSeq 3000/4000 instrument in single-end 50bp mode. RnBeads (30) were used for quality control and initial analysis of the DNA methylation data according to established practices (31). We summarized CpGs in 1,000 kb bins and performed differential DNA methylation analysis between ω-6 PUFA ($n = 3$) and control ($n = 6$) datasets using *limma* (32) (FDR-adjusted p-value < 0.05, fold change > 1.5, absolute difference > 25 percentage points). Locus overlap analysis (*LOLA*) (33) was used to calculate the relative overrepresentation of hypermethylated tiles with respect to three published ChIP-seq peak lists from its core database, corresponding to binding sites of *Stat3*, *c-Myb*, and C*ebpb* (34).

Chromatin accessibility. Open chromatin mapping was performed with the assay for transposase accessible chromatin (ATAC-seq) (35) with minor adaptations (36). In each experiment, 1x10 cells were incubated in the transposase reaction mix (12,5 µL 2× TD buffer, 2 µL T_N5 transposase (Illumina) 0,1% NP40 and 10,25 µL nuclease-free water) at 37 °C for 30 min. After DNA purification with the MinElute kit (Qiagen), 1 µl of the eluted DNA was used in a qPCR reaction to estimate the optimum number of amplification cycles. Library amplification was followed by a SPRI size-selection to exclude fragments larger than 1,200 bp. DNA concentration was measured with a Qubit fluorometer (Life Technologies). Sequencing was performed on an Illumina HiSeq 3000/4000 instrument in single-end 50bp mode. Raw sequencing data were trimmed using *Skewer* (37) followed by alignment to the GRCh38 assembly of the human reference genome with *Bowtie* (38) (parameters: --very-sensitive --no-discordant). Only deduplicated, uniquely mapped reads with mapping quality ≥30 were retained for further analysis. To identify accessible genome regions, we used *MACS2* (39) (parameters: -q 0.1 -g hs). Following initial data processing, all subsequent analyses were performed in R using Bioconductor packages. After removing peaks that overlapped blacklisted regions from the *ENCODE* consortium (34) and merging all overlapping 2-AG peaks, we quantified for each input dataset the number of reads in the retained peaks. Raw read counts were loaded into *DESeq2* (40) for normalization and differential analysis (FDR-adjusted p-value < 0.05). In our analysis, we used the sequencing flowcell as a covariate to account for batch effects. To further prevent disproportionate normalization between globally altered chromatin accessibility landscape (as observed between sample groups), we added random genome regions to the calculation step for the size factors of *DESeq2* (three times as many as actual peaks). We annotated each peak with the closest gene (distance relative to gene start coordinate based on Ensembl v77) and used *Enrichr* for functional enrichment analysis of differentially accessible regions (41).

Statistics. The number of independent samples is indicated in the graphs and the number of animals is indicated in the figure legends. All values represent the mean ± s.d. of independent experiments. Samples were tested for equal variance throughout. Statistically significant differences were determined by either Student's *t*-test (two-tailed for independent groups) or one-way analysis of variance (ANOVA) followed by Bonferroni's *post-hoc* test (for multiple groups). Statistical analysis was performed with Prism 6.0 (GraphPad Software Inc.). Statistical significance is indicated by asterisks (*$p < 0.05$, **$p < 0.01$, ***$p < 0.001$ and ****$p < 0.0001$).

Results

Dietary ω-6 PUFA enrichment during pregnancy impacts fetal cortical architecture

To test if fetal corticogenesis in mice undergoes life-long modifications after a prenatal diet enriched in ω-6 PUFAs, dams were fed a 'fast-food-like' hypercaloric diet with its ω-6 PUFA content increased through supplementation with linoleic acid and arachidonic acid (**Fig. S2a**) by ~15-fold (to ~31% of all fatty acids) while maintaining the ω-3:ω-6 ratio (**Table S1**), for either 2 weeks ('*priming protocol*'; **Fig. S2b**) or 8 weeks ('*programming protocol*'; **Fig. S2b$_1$**) prior to conception and during pregnancy. Besides their weight gain (**Fig. S2c**), ω-6 PUFA-fed dams had difficulties in conceiving (success rate of pregnancy: ~50% for both protocols *vs*. ~75% on control chow), and had fewer viable embryos (8 ± 1.08 (ω-6 PUFA) *vs*. 12 ± 1.2 (control)) but retained ~50% sex ratio.

Initially, dams in the 'programming protocol' were pulsed with 5-ethynyl-2′-deoxyuridine (EdU)(22) on embryonic day (E)14.5, which coincides with the peak of cortical neurogenesis (42), to address if ω-6 PUFAs modify the number and positions of new-born neurons destined to the cerebral cortex. In E18.5 fetuses, EdU^+ cells accumulated in the subventricular zone/deep cortical plate with a proportional decrease in neurons reaching the dorsal cortical plate/marginal zone that forms first in the outside-in hierarchy of cortical lamination (**Fig. 1a**) (42). These data were verified for both feeding protocols by histochemical detection of $Ki67^+$ neurons (**Fig. S3a**), and revealed a marked increase in $Ki67^+$ progenies at locations overlapping with the sites where EdU^+ cells had accumulated. EdU and Ki67 do not differentiate between radially-migrating pyramidal cells and interneurons commuting tangentially (42). Therefore, we used cholecystokinin $(CCK)^{BAC/DsRed}$ mice whose genetically-tagged $DsRed^+$ progeny are predominantly GABA interneurons (co-expressing *Gad1*, **Fig. S3b-b$_2$**) and populate the cerebral marginal zone (18). Both maternal feeding regimes led to a significant redistribution of $DsRed^+$ neurons with their loss in the marginal zone

(interneurons) and accumulation in deep cortical layers (likely pyramidal cells; **Fig. 1b** and **S3d,d$_1$**), establishing impaired cortical lamination upon maternal ω-6 PUFA enrichment. Next, axon-specific morphometry (18, 19) using neural cell adhesion molecule L1 (L1NCAM; **Fig. S3c**) revealed that corticofugal axons coalesced into enlarged fascicles that spread in the callosal primordium ('programming protocol'; **Fig. 1c,c$_1$**) in E18.5 fetuses whose mothers were on the ω-6 PUFA-enriched diet. This contrasted with control cases, which had corticofugal axons spaced evenly as fine-caliber fascicles (19, 43). These data suggest that maternal dietary choices during pregnancy carries a risk for fetal cortical abnormalities.

The misplacement of cortical neurons and their axonal defects observed upon hyperchaloric feeding regimes show striking similarities with failures of cortical wiring upon genetic (19, 43) and pharmacological (43) disruption of endocannabinoid signaling in the developing nervous system. This notion is particularly relevant since CCK$^+$ interneurons in the fetal cerebrum preferentially express CB$_1$Rs (9) and use endocannabinoids as focal cues for chemotaxis (**Fig. S1a,b**). Both linoleic acid and AA, available in excess in the hypercaloric diet (**Table S1**), can act as endocannabinoid precursors (**Fig. S2a**). This is compatible with altered AEA and 2-AG levels in fetal cerebrum (shown from the 'programming protocol'; **Fig. 1d**) with a shift favoring the availability of 2-AG, a full agonist at CB$_1$Rs, which we interpreted as a consequence of increased precursor bioavailability and processing. Desensitization of CB$_1$Rs together with the expressional deregulation of both the CB$_1$R and monoacylglycerol lipase (MAGL), the enzyme degrading the bulk of 2-AG in fetal brain (6, 43), is an effective means to impart a 'loss-of-function' signature on cortical architecture (19). Indeed, both CB$_1$Rs (**Fig. 1e** and **S4a**) and MAGL (**Fig. S4b**) showed >50% loss at the protein level with their mRNA transcripts unaffected (**Fig. S4c,d**), in fetuses from hyperchaloric diet-exposed dams, regardless of the length of the feeding protocol. Cumulatively, these data suggest that excess ω-6 PUFA intake increases endocannabinoid precursor availability and signaling to produce CB$_1$R inactivation over time, phenocopying mice with genetic *Cnr1* loss of function (19). The biological significance of AA-to-endocannabinoid conversion as a metabolic principle is reinforced by the AM251 sensitivity of neurite growth retardation upon AA supplementation (10 μM, **Fig. S1a,b**).

Dietary ω-6 PUFA enrichment reduces IgCAM expression in fetal cerebrum

We used isobaric tagging for relative and absolute quantitation (iTRAQ) (19) as a means to search for molecular determinants underpinning neuronal deficits. In E18.5 cerebri (including

cortical plate and dorsal hippocampus) (**Fig. 2a**), increased maternal intake of ω-6 PUFAs ('programming protocol') significantly altered the abundance of 208 proteins, which were assigned to 12 major functional clusters by gene ontology (**Fig. 2a$_1$**). Twelve proteins (6%) belonged to the cluster of '*cell adhesion/extracellular matrix composition*' (**Fig. 2a$_1$**). A refined analysis focusing on male embryos returned 215 proteins as significantly different, including 8 '*cell adhesion molecules*' (4%) as topmost male-specific targets: members of the immunoglobulin family of cell adhesion molecules (IgCAMs) (44) were coincidently and significantly down-regulated along with presynapse-specific synaptosomal-associated protein 25 (**Fig. 2a$_2$**), vesicle-associated membrane protein 2 and syntaxins (**Table S2**), indispensable for presynaptic neurotransmitter release at mature synapses.

Next, we focused on limbic system-associated membrane protein (*Lsamp*) because of its confinement to cortical structures in the dorsal telencephalon(45) (**Fig. S5a**) and interaction with other IgCAMs to regulate neurite outgrowth(46) (**Fig. S5b**). By combining qPCR (**Fig. 2b**) and Western blot analyses on subcellular fractions (**Fig. 2c**), we verified that heightened ω-6 PUFA intake, even for short periods, disrupted *Lsamp* mRNA and protein expression and subcellular localization. Notably, and even if its distribution is more general in the fetal hippocampus (**Fig. 2d-d$_4$**), *Lsamp* was invariably but not exclusively found around $CCK^{BAC/DsRed+}$ fetal interneurons (**Fig. 2d$_1$-d$_4$** and **S5c,d**) by E18.5, thus anatomically linking IgCAM deregulation to the differentiation and placement of CB_1R^+ cell populations (19, 43). We have genetically linked *Lsamp* expression to upstream CB_1R activity by demonstrating significantly reduced *Lsamp* mRNA expression in both *Cnr1*$^{-/-}$ fetuses (E18.5; **Fig. 2e**) and when exposing primary cortical neurons to AM251 (200 nM), a selective CB_1R antagonist (**Fig. 2f**). We could similarly implicate L1CAM, NCAM and neurotrimin, alternative members of the IgCAM family, in cortical deficits upon maternal ω-6 PUFA overfeeding because of their mRNA expression being significantly reduced by both 'priming' and 'programming' protocols (**Fig. 2g**) and upon CB_1R ablation (*Cnr1*$^{-/-}$; **Fig. 2h**). Overall, these data suggest that IgCAMs are molecular targets of CB_1R-mediated signal transduction cascades. Moreover, they qualify the transcriptional modification of IgCAMs as a candidate mechanism (**Fig. 3a**) through which maternal ω-6 PUFA preference impairs fetal brain development in male embryos, a hypothesis compatible with a role for endocannabinoids in axonal growth and directional guidance in the fetal cerebrum (43).

ω-6 PUFA enrichment reduces chromatin accessibility of transcription factors downstream from CB_1Rs

The design logic of CB_1R activity posits the recruitment of elaborate transcription factor networks with signal transducer and activator of transcription 3 (STAT3) being a prototypic effector to regulate CB_1R-dependent neurite outgrowth (47). Here, we reasoned that coincident expressional hindrances within the IgCAM family might indicate consensus transcription factor (TF) inactivation. By using publicly available gene expression microarray dat a(47) to select TF targets, we show that both 'priming' (**Fig. 3b**) and 'programming' protocols (**Fig. S6a**) significantly reduced the expression of *Stat3*, myeloblastosis oncogene (*Myb*) and CCAAT/enhancer-binding protein β (*Cebpb*) in fetal cortices (E18.5).

Next, we argued that long-lasting TF repression might be brought about by epigenetic modifications particularly since phytocannabinoids that engage CB_1Rs disrupt brain development by histone modifications (48). DNA methylation is a powerful means of gene regulation (49), which leaves the longest-lasting marks on chromatin. First, we performed genome-wide DNA methylation profiling in E18.5 fetal male brains after the 'priming' protocol and found broad gene repression along with CpG islands being hypermethylated. Second, enrichment analysis based on ChIP-seq data sets using the LOLA algorithm of genome-wide differences in DNA methylation revealed significant enrichments for the TFs STAT3, MYB and CEBPB in hypermethylated regions (**Fig. 3c**). Third, we used the assay of transposase-accessible chromatin (ATAC-seq), which is suitable to differentiate between effectively open (potentially active) and closed (potentially repressed) chromatin regions whilst also identifying the TFs that bind promoter regions of differential accessibility (50). To mechanistically link CB_1R activity and changes in the landscape of chromatin accessibility without confounds that could influence read-outs in protracted *in vivo* experiments, we performed ATAC-seq after treating primary cultures with 2-AG (5 μM) or AM251 (200 nM) for 7 days (**Fig. 3d**). Here, 2-AG reduced both *Lsamp* and *Stat3* mRNA expression, recapitulating our *in vivo* results (**Fig. 3e**; for AM251 see **Fig. S6b**). 1,423 genomic regions were identified with differential accessibility upon treatment, with decreased accessibility after both AM251 (**Fig. S6c**) and 2-AG exposures but with 2-AG showing higher effect amplitudes (**Fig. 3f**). This was particularly notable for the accessibility of the *Stat3* promoter (**Fig. 3g,g_1** and **S6d,d_1**). These observations were interpreted as 2-AG-induced receptor activation followed by permanent desensitization over 7 days (51). We then sought to gain broader insights in the biological relevance of signature regions with sensitivity to CB_1R-

mediated signaling by performing gene set enrichment analysis of all genes associated with differentially-accessible genomic loci using *Enrichr* (52). Based on ChIP-seq data available from the ENCODE project, an unexpectedly high fraction of the genomic loci losing accessibility upon 2-AG treatment occurred in the proximity of genes that are targets of TFs including BRCA1, FOS, CREB1 (**Fig. 3h** and **S6e**) that drive CB_1R-induced neurite outgrowth (43, 47). As such, their inactivation provides a transcriptional platform for endocannabinoid-induced axonal growth retardation upon CB_1R desensitization (**Fig. 3i** and **S6f**) (19, 43). Thus, our results outline an epigenetic regulatory framework to limit the transcription of gene sets underpinning neuronal morphogenesis upon long-lasting endocannabinoid excess.

Life-long effects of maternal ω-6 PUFA preference in first generation offspring

Epigenetic reprogramming of TF networks is biologically advantageous as a means to enforce genomic changes for as long as the lifetime of an organism (49). In accordance with this principle, we have assessed if key parameters of cortical reorganization endure into the adulthood of ω-6 PUFA-exposed offspring after programming feeding protocol. Firstly, AEA and 2-AG contents remained reflective of those in fetal brain, with significantly increased 2-AG levels detected on postnatal day 75 (**Fig. 4a**). At the same time, ω-6 PUFA-exposed offspring showed significantly reduced cortical CB_1R load (**Fig. 4b**), which we attribute to the presence of and adaptation to persistent 2-AG excess. Secondly, subcellular distribution of LSAMP, particularly its membrane-bound fraction, remained reduced (**Fig. 4c**), suggesting disrupted cell adhesion. Thirdly, genetic ablation of *Lsamp* provokes heightened behavioral responses to novel stressors in mice (53) and *Lsamp* gene polymorphisms correlate with depressive traits in humans (54). Therefore, we determined anxiety-like behaviors in the elevated plus-maze and open-field paradigms. Both tests revealed significant anxiety, reflected by shortened exploration of open surfaces (center of arena [**Fig. 4d**] and open arm entries [**Fig. 4e**]). Cumulatively, these data suggest that deregulated endocannabinoid signaling could contribute to the life-long manifestation of depression-like behaviors in mice born to dams consuming ω-6 PUFA-enriched chow during pregnancy. In agreement with our hypothesis that pre-conception and congenital excess of dietary ω-6 PUFAs and ensuing elevation of brain 2-AG levels cause the anxiety phenotype observed here, $Mgll^{-/-}$ mice (51), which lose the ability to hydrolyze endocannabinoids, exhibit chronic CB_1R desensitization and present anxiety-like behaviors. In contrast, life-long *n*-3-fatty acid deprivation impairs CB_1R-mediated synaptic signaling and emotional behavior in adulthood (55).

Discussion

In the present report we show transgenerational consequences of increasing the ω-6 PUFA nutritional content during pregnancy in mice on the development of the offsprings' nervous system. We outline that a critical mechanism involved is the engagement of the endocannabinoid system. As such, nutritional ω-6 PUFA-derived endocannabinoids desensitize CB_1Rs thereby altering neurogenesis, neuroblast commitment to the cerebral cortex and the formation of axonal connectivity. We suggest a link between long-lasting changes of cortical architecture and epigenetic repression of regulatory TF networks downstream from CB_1Rs that control neuronal differentiation (43, 47). The finding that many of the TF networks associated with axonal growth are epigenetically controlled by endocannabinoids might be relevant to public health in view of the ever-increasing world-wide pandemic of excess 'Western' diet and ensuing metabolic and behavioral dysfunctions (14).

A series of human longitudinal studies (and experimental reports) (12, 15) pinpoint optimal fatty acid composition in maternal diet during pregnancy as a means to reduce the risk of childhood diabetes, hypertension and obesity. Despite significant efforts in raising public awareness on the benefits of ω-3 PUFA-enriched diets ('fish' or 'Japanese' diets) for transgenerational disease prevention, the prevalence of dietary routines favoring ω-6 PUFAs is raising given easy access to high-fat fast food with extraordinary caloric composition. A reason for this is that intake of a concentrated source of dietary energy is considered rewarding particularly if it coincides with the intake of excess sugar or salt to raise flavor and aroma (56). Accordingly, preschool children born to mothers who preferred ω-3 PUFA-rich nutrients during pregnancy show higher cognitive scores (57) and are less prone to neurologic birth defects (58). In contrast, extreme pre-pregnancy weight is linked as a critical risk factor to attention deficit hyperactivity disorder (ADHD) (59), schizophrenia (60) and anxiety (61). Notably, the endocannabinoid system is a critical molecular component of the neuropathology of these neuropsychiatric disorders in both children and adults (62, 63) with an association between lowered CB_1R, CCK and GAD67 expression in cortical interneurons established as a key variable (64, 65). Our data are compatible with these considerations in humans, and provide a critical and causal link, at least in rodent models, between ω-6 PUFA-enriched diets during pregnancy and lactation, permanent neurochemical modifications that endure into adulthood and anxiety-like behaviors. Our *in vitro* finding that AA-to-endocannabinoid conversion is a cell-intrinsic metabolic feature is significant to emphasize

that not only systemic increases in circulating endocannabinoid levels but also excess endocannabinoid production *in situ* in developing organs could contribute to and diversify undesired ω-6 PUFA effects. Nevertheless, since AA is a precursor of a plethora of alternative bioactive products, many being essential for cell survival and function, we emphasize that balancing ω-3:ω-6 PUFA intake might be ultimately beneficial for neuronal development.

Even though our study focused on changes in the fetal nervous system, one ought to consider the constant interplay between the brain and peripheral organs through, e.g., long-range hormonal mechanisms. This notion is particularly relevant when studying the endocannabinoid system with its critical roles in the formation of e.g., bone (66), muscle (67), fat depots (68), immune system and pancreas (69) through recruitment of vastly different ligands and receptor systems. In obesity, CB_1R expression increases in multiple tissues (70) along with elevated circulating 2-AG levels as shown in both obese individuals (71) and in insulin-resistant obese postmenopausal women (72). Despite these inferences, we are acutely aware that the translational value of experimental data from laboratory rodents is often limited to human diseases. One confound we highlight is the C57Bl6/J strain used here, which is a favored laboratory subject due to its propensity to develop metabolic syndrome on high-fat diets (16, 68, 73). Nevertheless, the fact that both 2-AG and AEA concentrations are increased in the brain (16) and peripheral tissues (74) in conjunction with desensitization of brain CB_1Rs (16) in mice upon diet-induced obesity justify our choice of the animal model. Another concern is the timing and length of ω-6 PUFA administration because our experimental protocols precluded the pinpointing of a specific developmental window with peak sensitivity of the nervous system to imbalanced nutrient supply. A driving force behind our experimental design was that dietary preferences in humans are of long-lasting nature, often spanning years and decades. As such, the reduced probability of conception in obese females here is reminiscent of population data in humans (75), and lasts throughout pregnancy. Moreover, the metabolic multi-enzyme processing of ω-6 fatty acids is precisely controlled with brief exposures being well-tolerated and compensated. Therefore, an experimental design predisposing to heightened ω-6 PUFA levels in the long term is amenable for discovery research at the cellular and molecular levels.

In summary, we show that maternal dietary choices before and during pregnancy define brain development of the fetus, alike shown earlier for neonates and adolescents (13), and strongly influence epigenetic check-points that instruct neuronal differentiation.

Acknowledgements

We thank A. Reinthaler, for her expert laboratory assistance, A. Alpar and T. Hökfelt for discussions, the Biomedical Sequencing Facility at the Center for Molecular Medicine of the Austrian Academy of Sciences for assistance with next-generation sequencing, M. Watanabe (Hokkaido University) for antibodies, and A. Pimenta for technical help with LSAMP cytochemistry. GW Pharmaceuticals (UK) are acknowledged for providing access to an IncuCyte Zoom (Essen Bioscience) live-cell imaging platform. This work was supported by the Swedish Research Council (T.H.); Novo Nordisk Foundation (T.H.); Hjärnfonden (T.H.); European Research Council (SECRET-CELLS, ERC-2015-AdG-695136; T.H.), intramural funds of the Medical University of Vienna (T.H.) and the Wellcome Trust (grant number 094476/Z/10/Z, which funded the purchase of the TripleTOF 5600 mass spectrometer at the BSRC Mass Spectrometry and Proteomics Facility, University of St Andrews). M.F. is supported by a special research program of the Austrian Science Fund (FWF-F61).

Author contributions

TH conceived the project; VC, MF, CB, VDM, CJM, EK and TH designed experiments; CB, CJB and TH procured funding; VC, DC, MF, VG, MAF, FH, SLS, CHB and FP performed experiments; VC, DC, MF, FH, PP, FP analyzed data; ZM, GS and KM developed unique reagents and tools for the project and VC, MF and TH wrote the manuscript with input from all co-authors.

Conflict of interest

The authors declare that they have no conflict of interest.

Data availability

Proteomic data are being deposited in PRIDE with the accession number becoming available by final acceptance. Likewise, high-throughput sequencing data are being deposited with the Gene Expression Omnibus (GEO) accession number being available by final acceptance.

References

1. Schlingloff D, Kali S, Freund TF, Hajos N, Gulyas AI. Mechanisms of sharp wave initiation and ripple generation. The Journal of neuroscience : the official journal of the Society for Neuroscience. 2014 Aug 20;34(34):11385-98. PubMed PMID: 25143618.

2. Campbell K. Cortical neuron specification: it has its time and place. Neuron. 2005 May 5;46(3):373-6. PubMed PMID: 15882634.

3. Ayoub AE, Oh S, Xie Y, Leng J, Cotney J, Dominguez MH, et al. Transcriptional programs in transient embryonic zones of the cerebral cortex defined by high-resolution mRNA sequencing. Proceedings of the National Academy of Sciences of the United States of America. 2011 Sep 6;108(36):14950-5. PubMed PMID: 21873192. Pubmed Central PMCID: 3169109.

4. Bazinet RP, Laye S. Polyunsaturated fatty acids and their metabolites in brain function and disease. Nature reviews Neuroscience. 2014 Dec;15(12):771-85. PubMed PMID: 25387473.

5. Pfenninger KH. Plasma membrane expansion: a neuron's Herculean task. Nature reviews Neuroscience. 2009 Apr;10(4):251-61. PubMed PMID: 19259102.

6. Ahn K, McKinney MK, Cravatt BF. Enzymatic pathways that regulate endocannabinoid signaling in the nervous system. Chemical reviews. 2008 May;108(5):1687-707. PubMed PMID: 18429637. Pubmed Central PMCID: 3150828.

7. The nomenclature of lipids (recommendations 1976). IUPAC-IUB Commission on Biochemical Nomenclature. Journal of lipid research. 1978 Jan;19(1):114-28. PubMed PMID: 621435.

8. Bisogno T, Howell F, Williams G, Minassi A, Cascio MG, Ligresti A, et al. Cloning of the first sn1-DAG lipases points to the spatial and temporal regulation of endocannabinoid signaling in the brain. The Journal of cell biology. 2003 Nov 10;163(3):463-8. PubMed PMID: 14610053. Pubmed Central PMCID: 2173631.

9. Berghuis P, Rajnicek AM, Morozov YM, Ross RA, Mulder J, Urban GM, et al. Hardwiring the brain: endocannabinoids shape neuronal connectivity. Science. 2007 May 25;316(5828):1212-6. PubMed PMID: 17525344.

10. Keimpema E, Barabas K, Morozov YM, Tortoriello G, Torii M, Cameron G, et al. Differential subcellular recruitment of monoacylglycerol lipase generates spatial specificity of 2-arachidonoyl glycerol signaling during axonal pathfinding. The Journal of neuroscience : the official journal of the Society for Neuroscience. 2010 Oct 20;30(42):13992-4007. PubMed PMID: 20962221. Pubmed Central PMCID: 2987617.

11. Kirkham TC, Williams CM, Fezza F, Di Marzo V. Endocannabinoid levels in rat limbic forebrain and hypothalamus in relation to fasting, feeding and satiation: stimulation of eating by 2-arachidonoyl glycerol. British journal of pharmacology. 2002 Jun;136(4):550-7. PubMed PMID: 12055133. Pubmed Central PMCID: 1573386.

12. Simopoulos AP. Importance of the ratio of omega-6/omega-3 essential fatty acids: evolutionary aspects. World review of nutrition and dietetics. 2003;92:1-22. PubMed PMID: 14579680.

13. Manduca A, Bara A, Larrieu T, Lassalle O, Joffre C, Laye S, et al. Amplification of mGlu5-Endocannabinoid Signaling Rescues Behavioral and Synaptic Deficits in a Mouse Model of Adolescent and Adult Dietary Polyunsaturated Fatty Acid Imbalance. The Journal of neuroscience : the official journal of the Society for Neuroscience. 2017 Jul 19;37(29):6851-68. PubMed PMID: 28630250.

14. Stephenson J, Heslehurst N, Hall J, Schoenaker D, Hutchinson J, Cade JE, et al. Before the beginning: nutrition and lifestyle in the preconception period and its importance for

future health. Lancet. 2018 May 5;391(10132):1830-41. PubMed PMID: 29673873. Pubmed Central PMCID: 6075697.

15. Simopoulos AP. An Increase in the Omega-6/Omega-3 Fatty Acid Ratio Increases the Risk for Obesity. Nutrients. 2016 Mar 2;8(3):128. PubMed PMID: 26950145. Pubmed Central PMCID: 4808858.

16. Massa F, Mancini G, Schmidt H, Steindel F, Mackie K, Angioni C, et al. Alterations in the hippocampal endocannabinoid system in diet-induced obese mice. The Journal of neuroscience : the official journal of the Society for Neuroscience. 2010 May 5;30(18):6273-81. PubMed PMID: 20445053. Pubmed Central PMCID: 3636535.

17. Di Marzo V, Matias I. Endocannabinoid control of food intake and energy balance. Nature neuroscience. 2005 May;8(5):585-9. PubMed PMID: 15856067.

18. Calvigioni D, Mate Z, Fuzik J, Girach F, Zhang MD, Varro A, et al. Functional Differentiation of Cholecystokinin-Containing Interneurons Destined for the Cerebral Cortex. Cerebral cortex. 2017 Apr 1;27(4):2453-68. PubMed PMID: 27102657.

19. Tortoriello G, Morris CV, Alpar A, Fuzik J, Shirran SL, Calvigioni D, et al. Miswiring the brain: Delta9-tetrahydrocannabinol disrupts cortical development by inducing an SCG10/stathmin-2 degradation pathway. The EMBO journal. 2014 Apr 1;33(7):668-85. PubMed PMID: 24469251. Pubmed Central PMCID: 4000086.

20. Berghuis P, Dobszay MB, Wang X, Spano S, Ledda F, Sousa KM, et al. Endocannabinoids regulate interneuron migration and morphogenesis by transactivating the TrkB receptor. Proceedings of the National Academy of Sciences of the United States of America. 2005 Dec 27;102(52):19115-20. PubMed PMID: 16357196. Pubmed Central PMCID: 1323195.

21. Mulder J, Aguado T, Keimpema E, Barabas K, Ballester Rosado CJ, Nguyen L, et al. Endocannabinoid signaling controls pyramidal cell specification and long-range axon patterning. Proceedings of the National Academy of Sciences of the United States of America. 2008 Jun 24;105(25):8760-5. PubMed PMID: 18562289. Pubmed Central PMCID: 2438381.

22. Zeng C, Pan F, Jones LA, Lim MM, Griffin EA, Sheline YI, et al. Evaluation of 5-ethynyl-2'-deoxyuridine staining as a sensitive and reliable method for studying cell proliferation in the adult nervous system. Brain research. 2010 Mar 10;1319:21-32. PubMed PMID: 20064490. Pubmed Central PMCID: 2826567.

23. De Marchi N, De Petrocellis L, Orlando P, Daniele F, Fezza F, Di Marzo V. Endocannabinoid signalling in the blood of patients with schizophrenia. Lipids in health and disease. 2003 Aug 19;2:5. PubMed PMID: 12969514. Pubmed Central PMCID: 194767.

24. Matias I, Gonthier MP, Orlando P, Martiadis V, De Petrocellis L, Cervino C, et al. Regulation, function, and dysregulation of endocannabinoids in models of adipose and beta-pancreatic cells and in obesity and hyperglycemia. The Journal of clinical endocrinology and metabolism. 2006 Aug;91(8):3171-80. PubMed PMID: 16684820.

25. Walf AA, Frye CA. The use of the elevated plus maze as an assay of anxiety-related behavior in rodents. Nature protocols. 2007;2(2):322-8. PubMed PMID: 17406592. Pubmed Central PMCID: 3623971.

26. Harkany T, Mulder J, Sasvari M, Abraham I, Konya C, Zarandi M, et al. N-Methyl-D-aspartate receptor antagonist MK-801 and radical scavengers protect cholinergic nucleus basalis neurons against beta-amyloid neurotoxicity. Neurobiology of disease. 1999 Apr;6(2):109-21. PubMed PMID: 10343326.

27. Harkany T, O'Mahony S, Kelly JP, Soos K, Toro I, Penke B, et al. Beta-amyloid(Phe(SO3H)24)25-35 in rat nucleus basalis induces behavioral dysfunctions,

impairs learning and memory and disrupts cortical cholinergic innervation. Behavioural brain research. 1998 Feb;90(2):133-45. PubMed PMID: 9580273.

28. Sheffield NC, Pierron G, Klughammer J, Datlinger P, Schonegger A, Schuster M, et al. DNA methylation heterogeneity defines a disease spectrum in Ewing sarcoma. Nature medicine. 2017 Mar;23(3):386-95. PubMed PMID: 28134926. Pubmed Central PMCID: 5951283.

29. Klughammer J, Kiesel B, Roetzer T, Fortelny N, Nemc A, Nenning KH, et al. The DNA methylation landscape of glioblastoma disease progression shows extensive heterogeneity in time and space. Nature medicine. 2018 Oct;24(10):1611-24. PubMed PMID: 30150718. Pubmed Central PMCID: 6181207.

30. Assenov Y, Muller F, Lutsik P, Walter J, Lengauer T, Bock C. Comprehensive analysis of DNA methylation data with RnBeads. Nature methods. 2014 Nov;11(11):1138-40. PubMed PMID: 25262207. Pubmed Central PMCID: 4216143.

31. Bock C. Analysing and interpreting DNA methylation data. Nature reviews Genetics. 2012 Oct;13(10):705-19. PubMed PMID: 22986265.

32. Ritchie ME, Phipson B, Wu D, Hu Y, Law CW, Shi W, et al. limma powers differential expression analyses for RNA-sequencing and microarray studies. Nucleic acids research. 2015 Apr 20;43(7):e47. PubMed PMID: 25605792. Pubmed Central PMCID: 4402510.

33. Sheffield NC, Bock C. LOLA: enrichment analysis for genomic region sets and regulatory elements in R and Bioconductor. Bioinformatics. 2016 Feb 15;32(4):587-9. PubMed PMID: 26508757. Pubmed Central PMCID: 4743627.

34. Consortium EP. An integrated encyclopedia of DNA elements in the human genome. Nature. 2012 Sep 6;489(7414):57-74. PubMed PMID: 22955616. Pubmed Central PMCID: 3439153.

35. Buenrostro JD, Wu B, Chang HY, Greenleaf WJ. ATAC-seq: A Method for Assaying Chromatin Accessibility Genome-Wide. Current protocols in molecular biology. 2015 Jan 5;109:21 9 1-9. PubMed PMID: 25559105. Pubmed Central PMCID: 4374986.

36. Rendeiro AF, Schmidl C, Strefford JC, Walewska R, Davis Z, Farlik M, et al. Chromatin accessibility maps of chronic lymphocytic leukaemia identify subtype-specific epigenome signatures and transcription regulatory networks. Nature communications. 2016 Jun 27;7:11938. PubMed PMID: 27346425. Pubmed Central PMCID: 5494194.

37. Jiang H, Lei R, Ding SW, Zhu S. Skewer: a fast and accurate adapter trimmer for next-generation sequencing paired-end reads. BMC bioinformatics. 2014 Jun 12;15:182. PubMed PMID: 24925680. Pubmed Central PMCID: 4074385.

38. Langmead B, Salzberg SL. Fast gapped-read alignment with Bowtie 2. Nature methods. 2012 Mar 4;9(4):357-9. PubMed PMID: 22388286. Pubmed Central PMCID: 3322381.

39. Zhang Y, Liu T, Meyer CA, Eeckhoute J, Johnson DS, Bernstein BE, et al. Model-based analysis of ChIP-Seq (MACS). Genome biology. 2008;9(9):R137. PubMed PMID: 18798982. Pubmed Central PMCID: 2592715.

40. Love MI, Huber W, Anders S. Moderated estimation of fold change and dispersion for RNA-seq data with DESeq2. Genome biology. 2014;15(12):550. PubMed PMID: 25516281. Pubmed Central PMCID: 4302049.

41. Chen EY, Tan CM, Kou Y, Duan Q, Wang Z, Meirelles GV, et al. Enrichr: interactive and collaborative HTML5 gene list enrichment analysis tool. BMC bioinformatics. 2013 Apr 15;14:128. PubMed PMID: 23586463. Pubmed Central PMCID: 3637064.

42. Kepecs A, Fishell G. Interneuron cell types are fit to function. Nature. 2014 Jan 16;505(7483):318-26. PubMed PMID: 24429630. Pubmed Central PMCID: 4349583.

43. Maccarrone M, Guzman M, Mackie K, Doherty P, Harkany T. Programming of neural cells by (endo)cannabinoids: from physiological rules to emerging therapies. Nature reviews Neuroscience. 2014 Dec;15(12):786-801. PubMed PMID: 25409697. Pubmed Central PMCID: 4765324.

44. Cavallaro U, Dejana E. Adhesion molecule signalling: not always a sticky business. Nature reviews Molecular cell biology. 2011 Mar;12(3):189-97. PubMed PMID: 21346732.

45. Reinoso BS, Pimenta AF, Levitt P. Expression of the mRNAs encoding the limbic system-associated membrane protein (LAMP): I. Adult rat brain. The Journal of comparative neurology. 1996 Nov 11;375(2):274-88. PubMed PMID: 8915830.

46. Gil OD, Zhang L, Chen S, Ren YQ, Pimenta A, Zanazzi G, et al. Complementary expression and heterophilic interactions between IgLON family members neurotrimin and LAMP. Journal of neurobiology. 2002 Jun 5;51(3):190-204. PubMed PMID: 11984841.

47. Bromberg KD, Ma'ayan A, Neves SR, Iyengar R. Design logic of a cannabinoid receptor signaling network that triggers neurite outgrowth. Science. 2008 May 16;320(5878):903-9. PubMed PMID: 18487186. Pubmed Central PMCID: 2776723.

48. Szutorisz H, Hurd YL. Epigenetic Effects of Cannabis Exposure. Biological psychiatry. 2016 Apr 1;79(7):586-94. PubMed PMID: 26546076. Pubmed Central PMCID: 4789113.

49. Lowdon RF, Jang HS, Wang T. Evolution of Epigenetic Regulation in Vertebrate Genomes. Trends in genetics : TIG. 2016 May;32(5):269-83. PubMed PMID: 27080453. Pubmed Central PMCID: 4842087.

50. Buenrostro JD, Giresi PG, Zaba LC, Chang HY, Greenleaf WJ. Transposition of native chromatin for fast and sensitive epigenomic profiling of open chromatin, DNA-binding proteins and nucleosome position. Nature methods. 2013 Dec;10(12):1213-8. PubMed PMID: 24097267. Pubmed Central PMCID: 3959825.

51. Imperatore R, Morello G, Luongo L, Taschler U, Romano R, De Gregorio D, et al. Genetic deletion of monoacylglycerol lipase leads to impaired cannabinoid receptor CB(1)R signaling and anxiety-like behavior. Journal of neurochemistry. 2015 Nov;135(4):799-813. PubMed PMID: 26223500.

52. Farlik M, Halbritter F, Muller F, Choudry FA, Ebert P, Klughammer J, et al. DNA Methylation Dynamics of Human Hematopoietic Stem Cell Differentiation. Cell stem cell. 2016 Dec 1;19(6):808-22. PubMed PMID: 27867036. Pubmed Central PMCID: 5145815.

53. Catania EH, Pimenta A, Levitt P. Genetic deletion of Lsamp causes exaggerated behavioral activation in novel environments. Behavioural brain research. 2008 Apr 9;188(2):380-90. PubMed PMID: 18199495. Pubmed Central PMCID: 2275759.

54. Koido K, Traks T, Balotsev R, Eller T, Must A, Koks S, et al. Associations between LSAMP gene polymorphisms and major depressive disorder and panic disorder. Translational psychiatry. 2012 Aug 14;2:e152. PubMed PMID: 22892717. Pubmed Central PMCID: 3432189.

55. Lafourcade M, Larrieu T, Mato S, Duffaud A, Sepers M, Matias I, et al. Nutritional omega-3 deficiency abolishes endocannabinoid-mediated neuronal functions. Nature neuroscience. 2011 Mar;14(3):345-50. PubMed PMID: 21278728.

56. Drewnowski A. Energy intake and sensory properties of food. The American journal of clinical nutrition. 1995 Nov;62(5 Suppl):1081S-5S. PubMed PMID: 7484925.

57. Helland IB, Smith L, Saarem K, Saugstad OD, Drevon CA. Maternal supplementation with very-long-chain n-3 fatty acids during pregnancy and lactation augments children's IQ at 4 years of age. Pediatrics. 2003 Jan;111(1):e39-44. PubMed PMID: 12509593.

58. Crawford MA, Golfetto I, Ghebremeskel K, Min Y, Moodley T, Poston L, et al. The potential role for arachidonic and docosahexaenoic acids in protection against some central nervous system injuries in preterm infants. Lipids. 2003 Apr;38(4):303-15. PubMed PMID: 12848275.

59. Rodriguez A, Miettunen J, Henriksen TB, Olsen J, Obel C, Taanila A, et al. Maternal adiposity prior to pregnancy is associated with ADHD symptoms in offspring: evidence from three prospective pregnancy cohorts. International journal of obesity. 2008 Mar;32(3):550-7. PubMed PMID: 17938639.

60. Schaefer CA, Brown AS, Wyatt RJ, Kline J, Begg MD, Bresnahan MA, et al. Maternal prepregnant body mass and risk of schizophrenia in adult offspring. Schizophrenia bulletin. 2000;26(2):275-86. PubMed PMID: 10885630.

61. Rodriguez A. Maternal pre-pregnancy obesity and risk for inattention and negative emotionality in children. Journal of child psychology and psychiatry, and allied disciplines. 2010 Feb;51(2):134-43. PubMed PMID: 19674195.

62. Parolaro D, Realini N, Vigano D, Guidali C, Rubino T. The endocannabinoid system and psychiatric disorders. Experimental neurology. 2010 Jul;224(1):3-14. PubMed PMID: 20353783.

63. Lafenetre P, Chaouloff F, Marsicano G. Bidirectional regulation of novelty-induced behavioral inhibition by the endocannabinoid system. Neuropharmacology. 2009 Dec;57(7-8):715-21. PubMed PMID: 19607846.

64. Eggan SM, Stoyak SR, Verrico CD, Lewis DA. Cannabinoid CB1 receptor immunoreactivity in the prefrontal cortex: Comparison of schizophrenia and major depressive disorder. Neuropsychopharmacology : official publication of the American College of Neuropsychopharmacology. 2010 Sep;35(10):2060-71. PubMed PMID: 20555313. Pubmed Central PMCID: 2967726.

65. Eggan SM, Hashimoto T, Lewis DA. Reduced cortical cannabinoid 1 receptor messenger RNA and protein expression in schizophrenia. Archives of general psychiatry. 2008 Jul;65(7):772-84. PubMed PMID: 18606950. Pubmed Central PMCID: 2890225.

66. Ross RA. The enigmatic pharmacology of GPR55. Trends in pharmacological sciences. 2009 Mar;30(3):156-63. PubMed PMID: 19233486.

67. Iannotti FA, Silvestri C, Mazzarella E, Martella A, Calvigioni D, Piscitelli F, et al. The endocannabinoid 2-AG controls skeletal muscle cell differentiation via CB1 receptor-dependent inhibition of Kv7 channels. Proceedings of the National Academy of Sciences of the United States of America. 2014 Jun 17;111(24):E2472-81. PubMed PMID: 24927567. Pubmed Central PMCID: 4066524.

68. Ruiz de Azua I, Mancini G, Srivastava RK, Rey AA, Cardinal P, Tedesco L, et al. Adipocyte cannabinoid receptor CB1 regulates energy homeostasis and alternatively activated macrophages. The Journal of clinical investigation. 2017 Nov 1;127(11):4148-62. PubMed PMID: 29035280. Pubmed Central PMCID: 5663356.

69. Malenczyk K, Keimpema E, Piscitelli F, Calvigioni D, Bjorklund P, Mackie K, et al. Fetal endocannabinoids orchestrate the organization of pancreatic islet microarchitecture. Proceedings of the National Academy of Sciences of the United States of America. 2015 Nov 10;112(45):E6185-94. PubMed PMID: 26494286. Pubmed Central PMCID: 4653226.

70. Pagotto U, Vicennati V, Pasquali R. The endocannabinoid system and the treatment of obesity. Annals of medicine. 2005;37(4):270-5. PubMed PMID: 16019725.

71. Bluher M, Engeli S, Kloting N, Berndt J, Fasshauer M, Batkai S, et al. Dysregulation of the peripheral and adipose tissue endocannabinoid system in human abdominal obesity. Diabetes. 2006 Nov;55(11):3053-60. PubMed PMID: 17065342. Pubmed Central PMCID: 2228260.

72. Abdulnour J, Yasari S, Rabasa-Lhoret R, Faraj M, Petrosino S, Piscitelli F, et al. Circulating endocannabinoids in insulin sensitive vs. insulin resistant obese postmenopausal women. A MONET group study. Obesity. 2014 Jan;22(1):211-6. PubMed PMID: 23616305.

73. Gallou-Kabani C, Vige A, Gross MS, Rabes JP, Boileau C, Larue-Achagiotis C, et al. C57BL/6J and A/J mice fed a high-fat diet delineate components of metabolic syndrome. Obesity. 2007 Aug;15(8):1996-2005. PubMed PMID: 17712117.

74. Alvheim AR, Malde MK, Osei-Hyiaman D, Lin YH, Pawlosky RJ, Madsen L, et al. Dietary linoleic acid elevates endogenous 2-AG and anandamide and induces obesity. Obesity. 2012 Oct;20(10):1984-94. PubMed PMID: 22334255. Pubmed Central PMCID: 3458187.

75. Guelinckx I, Devlieger R, Beckers K, Vansant G. Maternal obesity: pregnancy complications, gestational weight gain and nutrition. Obesity reviews : an official journal of the International Association for the Study of Obesity. 2008 Mar;9(2):140-50. PubMed PMID: 18221480.

Legends to Figures

Fig. 1. ω-6 PUFA-enriched diets modulate cell migration by disengaging the endocannabinoid system. a,b, Representative images (*left*) and quantification (*right*) of EdU^+ (**a**; '*programming protocol*') and $CCK^{BAC/DsRed+}$ (**b**; '*priming protocol*') neurons in cortical layers of male embryos at E18.5. Cell counts were performed on equal cortical tissue surfaces in equal binned players (numbered consecutively from 1 to 10), and expressed as absolute numbers. **Figure S3** is referred to for direct comparisons of the two maternal feeding protocols with regards to their impact on cortical reorganization in the offspring. *Scale bars* = 20 μm. *Abbreviations:* cp, cortical plate; mz, marginal zone; svz, subventricular zone. **c,c$_1$**, Immunofluorescence histochemistry and quantification of the transverse diameter (c_1) of first-order axonal fascicles in male E18.5 embryos, labeled for L1NCAM, in the cortical intermediate zone after nutrient-induced reprogramming. **d**, Anandamide (AEA) and 2-AG levels in E18.5 cerebral tissue of mice (both sexes) after the '*programming*' protocol. **e**, Western analysis of CB_1R protein levels in E18.5 cerebral tissue of mixed sexes after both maternal priming (Pri) and programming (Pro) feeding protocols. Total protein load was visualized by Cy5 dye reagent and used to normalize CB_1R expression at 53 kDa (*arrow*). Quantitative data are shown to the right. (*$p < 0.05$, **$p < 0.01$, $n = 5$ mice/group. Data are means ± s.d. from three independent experiments.

Fig. 2. Dietary ω-6 PUFA enrichment reduces IgCAM expression in fetal cerebrum. a-a$_2$, Origin of cortical tissue ($n = 4$ biological replicates/group) used for quantitative iTRAQ proteomics (**a**), ontology classification of significantly altered proteins in mixed sex embryos through primary function assignment (**a$_1$**) and topmost modified protein targets (ω-6 PUFA-enriched diet *vs*. control) obtained after the '*programming*' protocol in male embryos (**a$_2$**). **b,** *Lsamp* mRNA expression after either the '*priming*' (Pri) or the '*programming*' (Pro) protocol in fetal cortices on E18.5. mRNAs were quantified by qPCR and normalized to *Gapdh* as a housekeeping standard. Data were expressed relative to fetuses from pregnancies on control chow. **c**, Western analysis of LSAMP in subcellular fractions (cytosol [cyto]; membrane fraction [MF]) of fetal cerebral tissues after '*programming*' protocol. **d-d$_4$**, Representative image of LSAMP immunoreactivity (**d$_1$**), particularly in the proximity of CCK^+ interneurons (**d$_2$**), in E18.5 hippocampi of $CCK^{BAC/DsRed}$ mice. **e,f,** *Lsamp* mRNA in *Cnr1*$^{-/-}$ cortices (**e**) and in E18.5 cortical neurons treated with AM251 for 96h (f). **g,h,** IgCAM mRNA levels after both '*priming*' and '*programming*' protocols (g) and in *Cnr1*$^{-/-}$ cortical tissue on E18.5 (h). mRNA expression was normalized to Gapdh. Lsamp expression was normalized to control-fed (c,g) or wild-type (e,h) mice. All data are on male mice. *Abbreviations:* CA1, cornu

Ammonis subfield 1; cng, cingulate cortex; Cpu, caudate putamen; DG dentate gyrus; f, fimbria; Ht, hypothalamus; Ntm, neurotrimin; sctx, somatosensory cortex; Th, thalamus. *Scale bars* = 75 μm (d), 8 μm (d, *inset*). *$p < 0.05$, **$p < 0.01$, $n = 3$ mice/group. Data are means ± s.d. from triplicate experiments.

Fig. 3. ω-6 PUFA-enriched diets reduce chromatin accessibility of transcription factors regulated by CB_1R activation. a, Schematic representation of signaling events and interactions. Grey color indicates the site of action for AM251 used for pharmacological probing. **b,** *Stat3*, *c-Myb* and *Cebpb* transcription factor mRNA levels in E18.5 cortical tissue ('*priming protocol*'). mRNAs were quantified by qPCR and normalized to *Gapdh*. Expression was normalized to control mice. *$p < 0.05$, $n = 3$ mice/group. **c,** Bar graph showing the relative enrichment of overlaps of transcription factor binding sites and genomic regions (1kb tiles) with increased DNA methylation in E18.5 cortical tissue upon excess ω-6 PUFA exposure ('*priming protocol*'). *LOLA* was used to test the enrichment of the three selected transcription factors using published ChIP-seq peaks from ENCODE and CODEX. *$p < 0.05$, **$p < 0.01$, $n = 3$ mice/group. **d,** Timeline of *in vitro* CB_1R agonist (2-AG, 5 μM) and antagonist (AM251, 200 nM see also SI Fig. 6) exposure. DIV = day *in vitro*. *$p < 0.05$, Data were expressed as means ± s.d. from three independent experiments. **e,** *Lsamp* and *Stat3* mRNAs in E18.5 primary cortical neurons after 2-AG (5 μM) exposure. mRNA expression (relative to *Gapdh*) was normalized to control. **f,** Heatmap of ATAC-seq data showing decreased chromatin accessibility after 2-AG treatment. Numbers denote the normalized and scaled read count per ATAC-seq peak. R1-R6 for both control and 2-AG treatments identify biological replicates from two independent experiments. **g-g_1**, Genome browser plot showing ATAC-seq signal intensity across cortical neurons in the vicinity of the *Stat3* gene after 2-AG application, and relative quantification (g_1). *DeSeq2*-normalized read counts. **h,** Enrichment analysis for all differentially accessible regions determined using *Enrichr*. ****$p < 0.0001$. **i**, Dynamic time-course analysis of neurite outgrowth after 2-AG exposure for 7 days aided by an IncuCyte automated imaging system. **$p < 0.01$, ****$p < 0.0001$. Data represent means ± s.d. from three independent experiments. All *in vivo* and *in vitro* data are on male mice. An equivalent dataset on tissues from the '*programming protocol*' at E18.5 is shown in SI Fig. 6.

Fig. 4. Life-long effects of maternal ω-6 PUFA preference in first generation offspring. **a**, Anandamide (AEA) and 2-AG levels in cortical tissues of mixed sexes on postnatal day

(PND) 75 after exposure to the 'programming' protocol. $^{**}p < 0.01$, n = 3-4 mice/group. **b,c**, Western analysis of CB_1R (**b**) and LSAMP (**c**) protein load in cerebral tissue of mixed sexes. CB_1R was enriched in membrane fractions, while LSAMP was detected in both the cytosol (cyto) and membranes (mf). Quantitative data are from triplicate experiments. **d,** Open-field behaviors of male mice born to and weaned from the '*programming protocol*', including the total distance travelled (m), the time spent (s) in the center of the arena and the velocity of movement (cm/s). $^{*}p < 0.05$, n = 4 mice/group. **e**, Elevated plus-maze behaviors of male offspring, such as the distance travelled (cm) on, the time spent (s) in and the number of entries (n) into open arms. $^{*}p < 0.05$, $^{**}p < 0.01$, n = 4 mice/group.

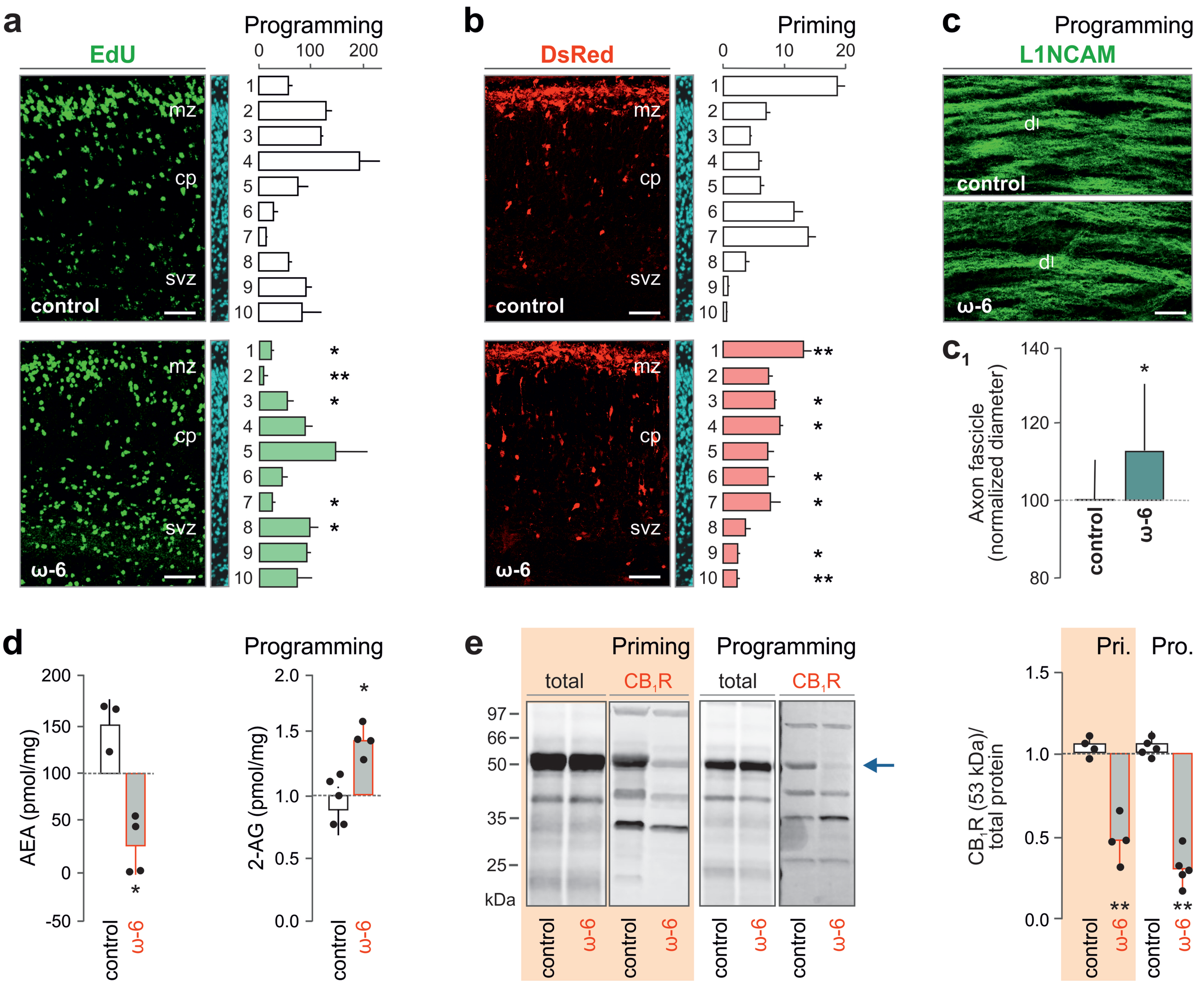
a
EdU
Programming
0
100
200
mz
cp
svz
control
ω-6
1
2
3
4
5
6
7
8
9
10
*
**
b
DsRed
Priming
0
10
20
c
L1NCAM
dl
control
ω-6
c1
Axon fasciculation
(normalized diameter)
140
120
100
80
d
AEA (pmol/mg)
200
150
100
50
0
-50
2-AG (pmol/mg)
2.0
1.5
1.0
0.5
0.0
e
total
CB1R
97
66
50
35
25
kDa
Pri.
Pro.
CB1R (53 kDa)/
total protein

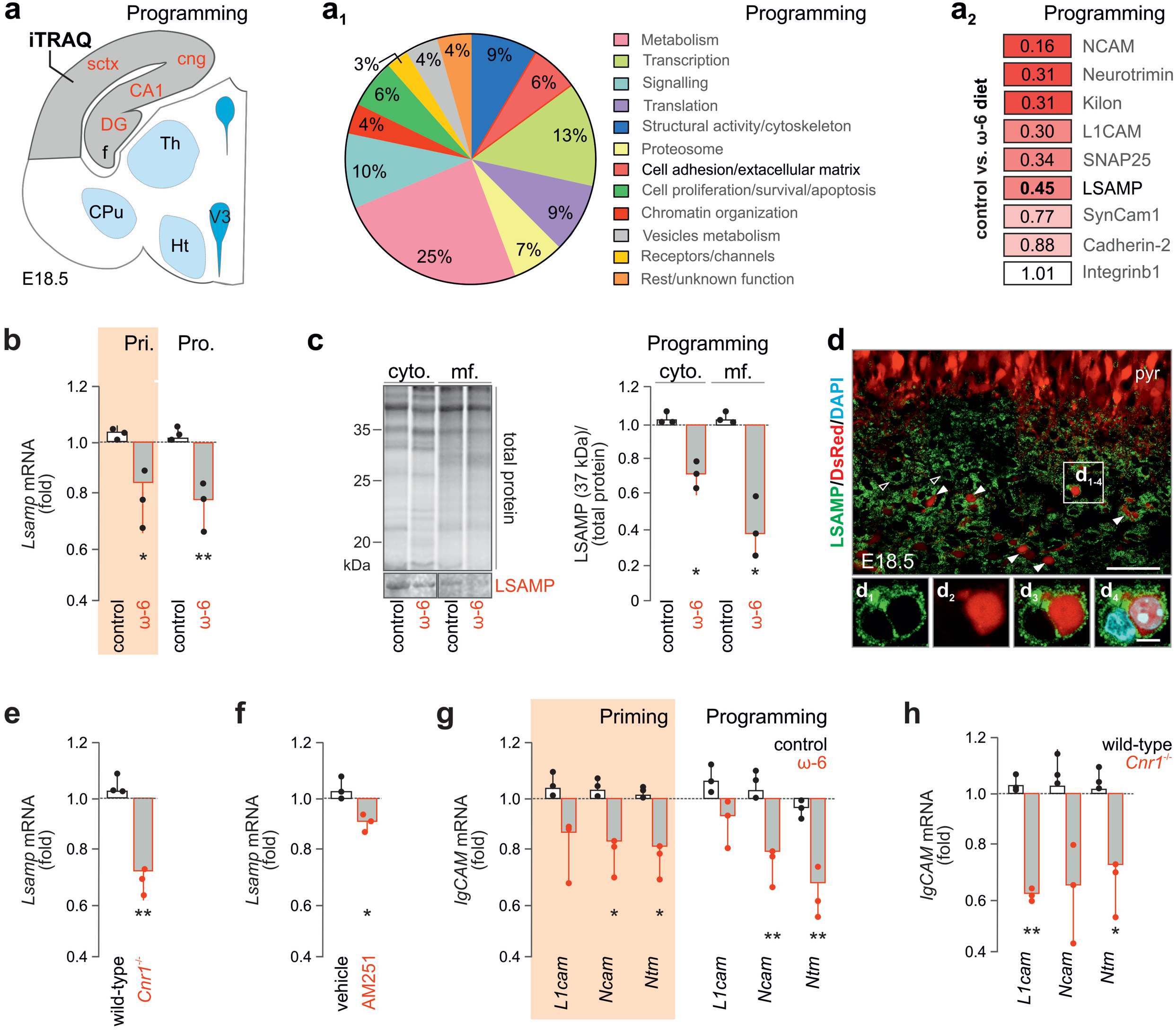
a
Programming
iTRAQ
sctx
cng
CA1
DG
f
Th
CPu
V3
Ht
E18.5
a1
Programming
3%
4%
4%
9%
6%
6%
4%
13%
10%
9%
25%
7%
Metabolism
Transcription
Signalling
Translation
Structural activity/cytoskeleton
Proteosome
Cell adhesion/extacellular matrix
Cell proliferation/survival/apoptosis
Chromatin organization
Vesicles metabolism
Receptors/channels
Rest/unknown function
a2
Programming
control vs. ω-6 diet
0.16 NCAM
0.31 Neurotrimin
0.31 Kilon
0.30 L1CAM
0.34 SNAP25
0.45 LSAMP
0.77 SynCam1
0.88 Cadherin-2
1.01 Integrinb1
b
Pri.
Pro.
Lsamp mRNA (fold)
1.2
1.0
0.8
0.6
0.4
*
**
control
ω-6
control
ω-6
c
cyto.
mf.
35
25
20
kDa
total protein
LSAMP
control
ω-6
control
ω-6
Programming
cyto.
mf.
LSAMP (37 kDa)/ (total protein)
1.2
1.0
0.8
0.6
0.4
0.2
0
*
*
control
ω-6
control
ω-6
d
pyr
LSAMP/DsRed/DAPI
d1-4
E18.5
d1
d2
d3
d4
e
Lsamp mRNA (fold)
1.2
1.0
0.8
0.6
0.4
**
wild-type
Cnr1-/-
f
Lsamp mRNA (fold)
1.2
1.0
0.8
0.6
0.4
*
vehicle
AM251
g
Priming
Programming
control
ω-6
IgCAM mRNA (fold)
1.2
1.0
0.8
0.6
0.4
*
*
**
**
L1cam
Ncam
Ntm
L1cam
Ncam
Ntm
h
wild-type
Cnr1-/-
IgCAM mRNA (fold)
1.2
1.0
0.8
0.6
0.4
**
*
L1cam
Ncam
Ntm

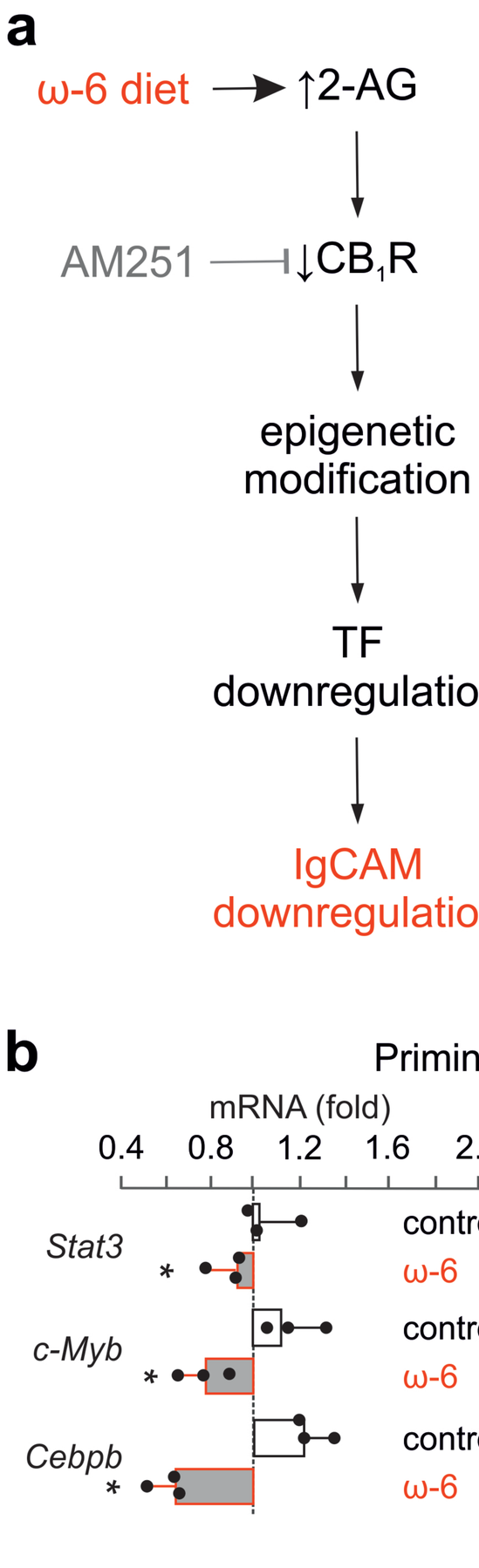
a
ω-6 diet
↑2-AG
AM251
↓CB1R
epigenetic modification
TF downregulation
IgCAM downregulation

b
Priming
mRNA (fold)
0.4
0.8
1.2
1.6
2.0
Stat3
c-Myb
Cebpb
control
ω-6
*

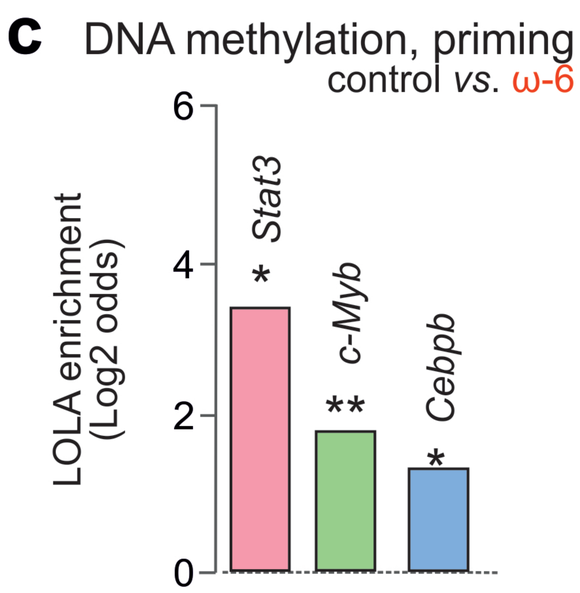
c
DNA methylation, priming
control vs. ω-6
LOLA enrichment (Log2 odds)
Stat3
c-Myb
Cebpb
*
**

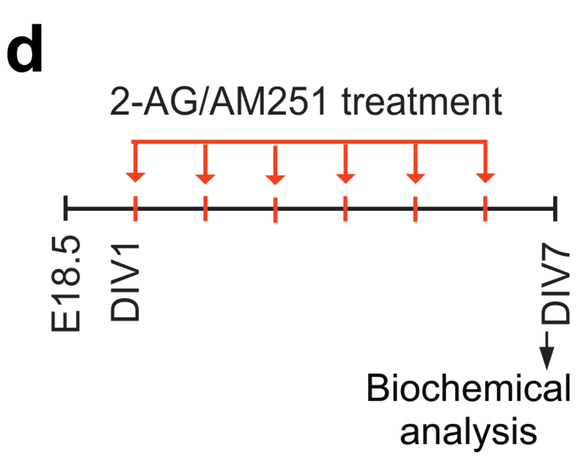
d
2-AG/AM251 treatment
E18.5
DIV1
DIV7
Biochemical analysis

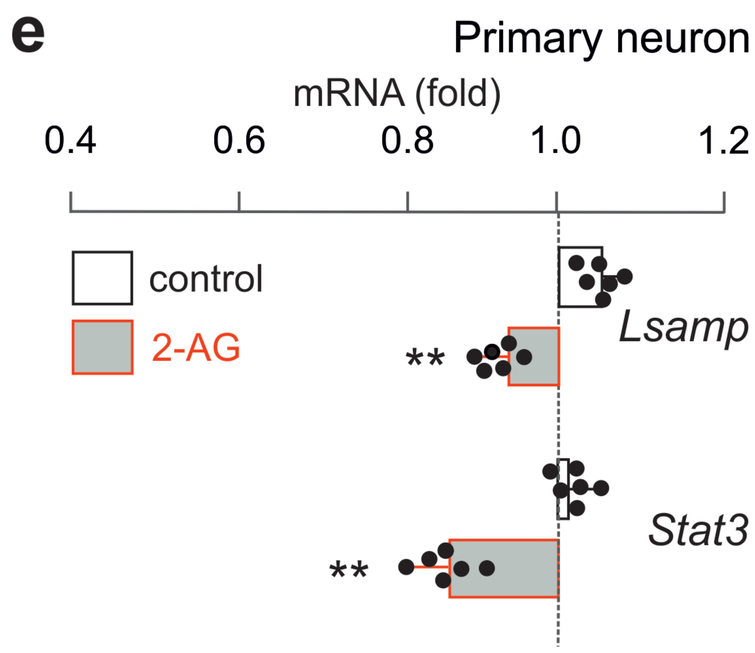
e
Primary neuron
mRNA (fold)
0.4
0.6
0.8
1.0
1.2
control
2-AG
Lsamp
Stat3
**

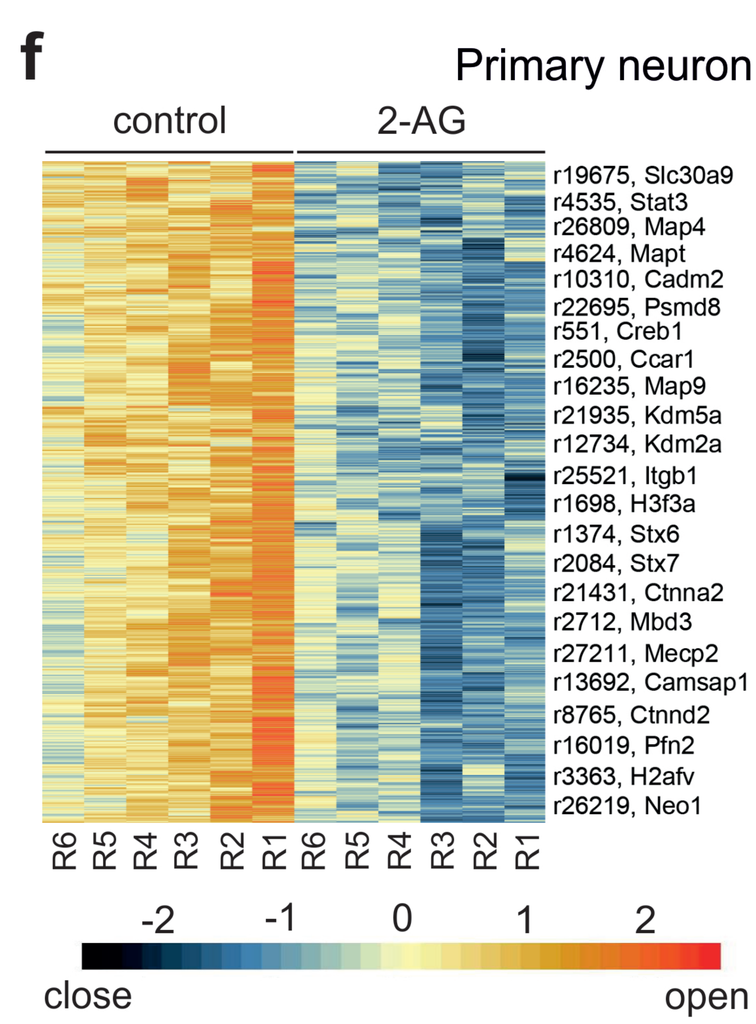
f
Primary neuron
control
2-AG
r19675, Slc30a9
r4535, Stat3
r26809, Map4
r4624, Mapt
r10310, Cadm2
r22695, Psmd8
r551, Creb1
r2500, Ccar1
r16235, Map9
r21935, Kdm5a
r12734, Kdm2a
r25521, Itgb1
r1698, H3f3a
r1374, Stx6
r2084, Stx7
r21431, Ctnna2
r2712, Mbd3
r27211, Mecp2
r13692, Camsap1
r8765, Ctnnd2
r16019, Pfn2
r3363, H2afv
r26219, Neo1
R6 R5 R4 R3 R2 R1 R6 R5 R4 R3 R2 R1
-2 -1 0 1 2
close
open

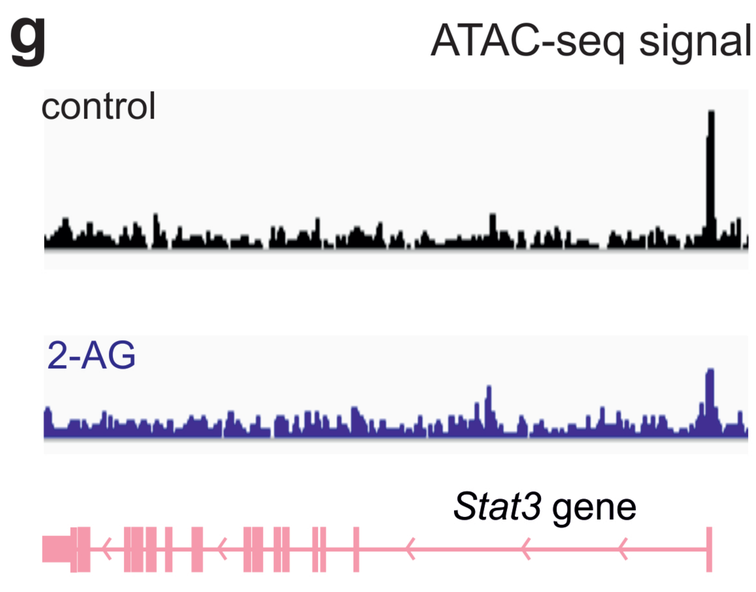
g
ATAC-seq signal
control
2-AG
Stat3 gene

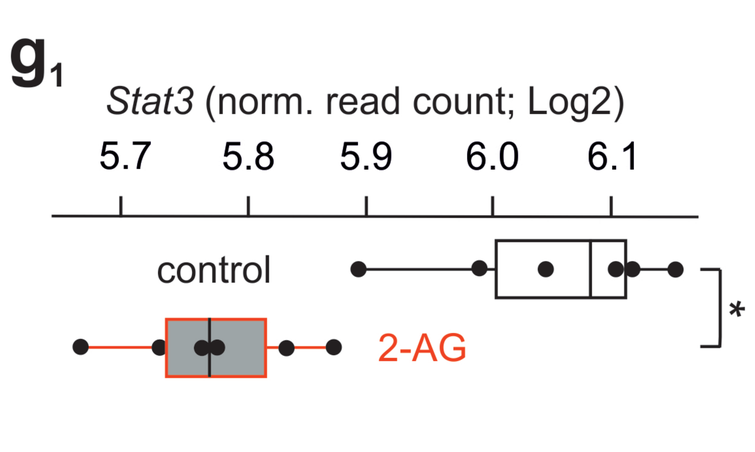
g1
Stat3 (norm. read count; Log2)
5.7
5.8
5.9
6.0
6.1
control
2-AG
*

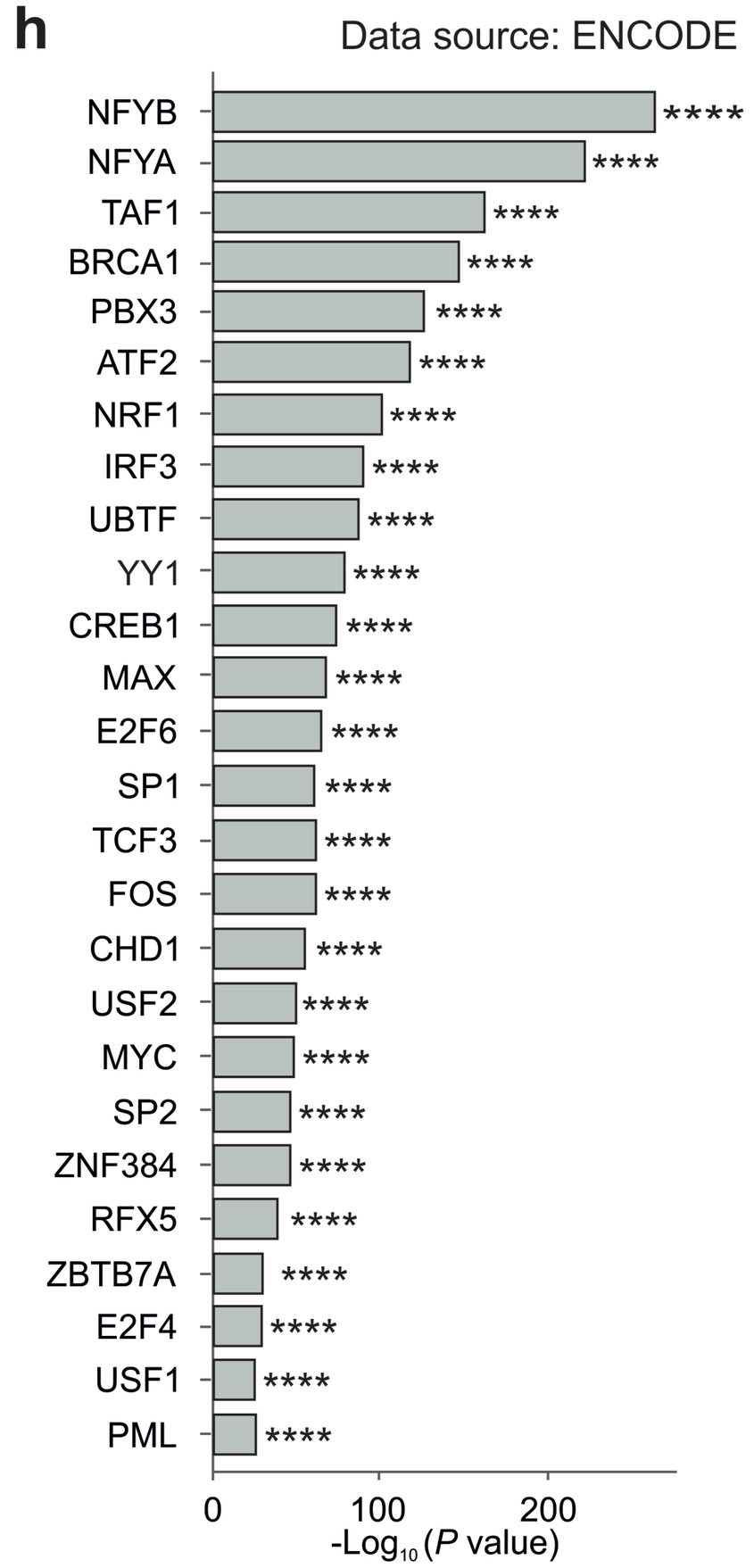
h
Data source: ENCODE
NFYB
NFYA
TAF1
BRCA1
PBX3
ATF2
NRF1
IRF3
UBTF
YY1
CREB1
MAX
E2F6
SP1
TCF3
FOS
CHD1
USF2
MYC
SP2
ZNF384
RFX5
ZBTB7A
E2F4
USF1
PML
****
0
100
200
-Log10 (P value)

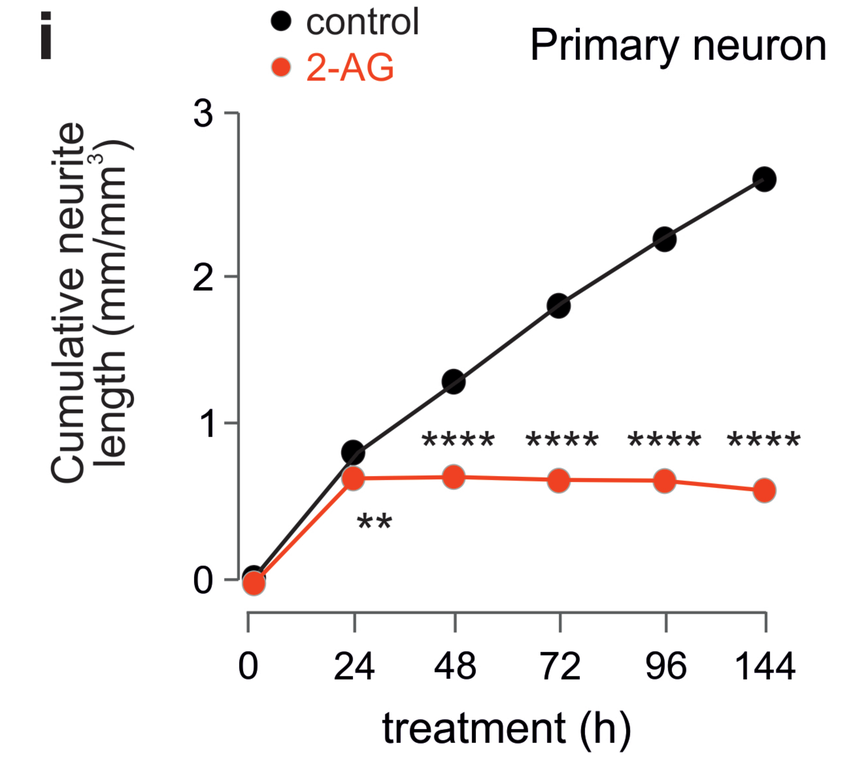
i
control
2-AG
Primary neuron
Cumulative neurite length (mm/mm3)
0
1
2
3
0
24
48
72
96
144
treatment (h)
**
****

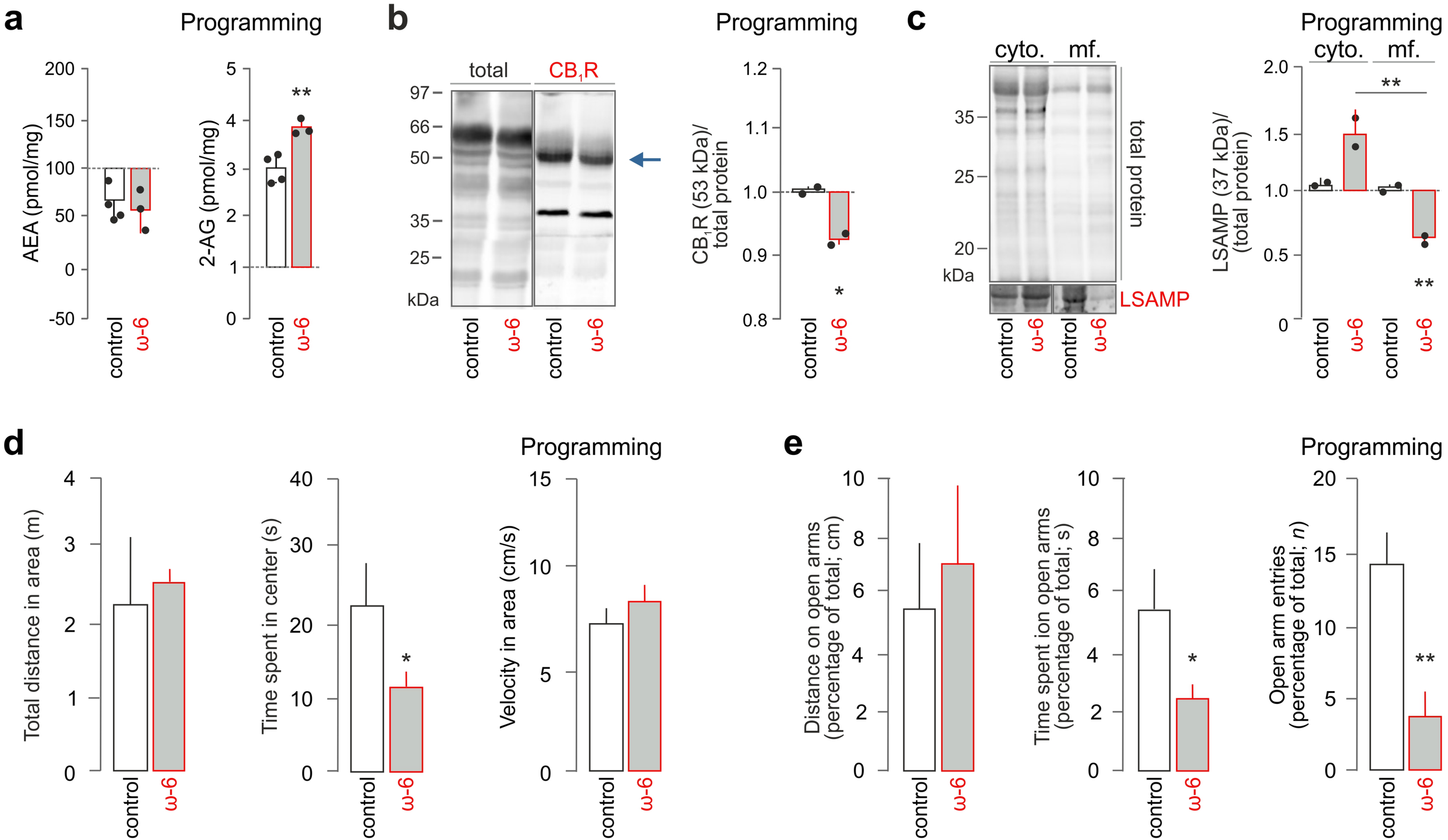
a
Programming
AEA (pmol/mg)
200
150
100
50
0
-50
control
ω-6
2-AG (pmol/mg)
5
4
3
2
1
0
**
control
ω-6
b
total
CB1R
97
66
50
35
25
kDa
control
ω-6
control
ω-6
Programming
CB1R (53 kDa)/ total protein
1.2
1.1
1.0
0.9
0.8
*
control
ω-6
c
cyto.
mf.
35
25
20
kDa
total protein
LSAMP
control
ω-6
control
ω-6
Programming
cyto.
mf.
LSAMP (37 kDa)/ (total protein)
2.0
1.5
1.0
0.5
0
**
**
control
ω-6
control
ω-6
d
Programming
Total distance in area (m)
4
3
2
1
0
control
ω-6
Time spent in center (s)
40
30
20
10
0
*
control
ω-6
Velocity in area (cm/s)
15
10
5
0
control
ω-6
e
Programming
Distance on open arms (percentage of total; cm)
10
8
6
4
2
0
control
ω-6
Time spent ion open arms (percentage of total; s)
10
8
6
4
2
0
*
control
ω-6
Open arm entries (percentage of total; n)
20
15
10
5
0
**
control
ω-6